

Footprint Characteristics Revised for Field-Scale Soil Moisture Monitoring with Cosmic-Ray Neutrons

M. Köhli,^{1,3} M. Schrön,^{2,3} M. Zreda,⁴ U. Schmidt,¹ P. Dietrich,² S. Zacharias²

Corresponding author: Martin Schrön, (martin.schroen@ufz.de)

¹Physikalisches Institut, Heidelberg

University,

²Department of Monitoring and

Exploration Technologies, UFZ - Helmholtz

Centre of Environmental Research, Leipzig,

³These authors contributed equally to this work,

⁴Department of Hydrology and Water

Resources, University of Arizona.

arXiv:1602.04469v1 [physics.geo-ph] 14 Feb 2016

Abstract. Cosmic-ray neutron probes are widely used to monitor environmental water content near the surface. The method averages over tens of hectares and is unrivaled in serving representative data for agriculture and hydrological models at the hectometer scale. Recent experiments, however, indicate that the sensor response to environmental heterogeneity is not fully understood. Knowledge of the support volume is a prerequisite for the proper interpretation and validation of hydrogeophysical data. In a previous study, several physical simplifications have been introduced into a neutron transport model in order to derive the characteristics of the cosmic-ray probe's footprint. We utilize a refined source and energy spectrum for cosmic-ray neutrons and simulate their response to a variety of environmental conditions. Results indicate that the method is particularly sensitive to soil moisture in the first tens of meters around the probe, whereas the radial weights are changing dynamically with ambient water. The footprint radius ranges from 130 to 240 m depending on air humidity, soil moisture and vegetation. The moisture-dependent penetration depth of 15 to 83 cm decreases exponentially with distance to the sensor. However, the footprint circle remains almost isotropic in complex terrain with nearby rivers, roads or hill slopes. Our findings suggest that a dynamically weighted average of point measurements is essential for accurate calibration and validation. The new insights will have important impact on signal interpretation, sensor installation, data interpolation from mobile surveys, and the choice of appropriate resolutions for data assimilation into hydrological models.

An edited version of this paper was published by AGU. Copyright 2015 American Geophysical Union.

M. Köhli, M. Schrön, et al., (2015), Water Resources Research, 51, 5772-5790,

DOI 10.1002/2015WR017169.

1. Introduction

Whenever hydrology, agriculture, or climate science are concerned, the endeavour to find efficient methods of quantifying water resources is vitally important. Extensive monitoring of soil moisture and above-ground water storage is of key importance to constrain hydrological model predictions or to control management systems for irrigation. However, small-scale variability of soil moisture has always been an issue for the interpretation and application of point measurements [Vereecken *et al.*, 2008; Biswas, 2014]. At large scales, remote sensing methods provide near-surface estimates of soil-moisture. However, drawbacks are shallow penetration depth, low temporal resolution and significant influence of surface conditions [e.g. Wagner *et al.*, 2007]. From the modeler’s perspective, information at scales other than the modeling scale requires procedures for rescaling which introduce uncertainty during the assimilation process [Vereecken *et al.*, 2007].

The method of cosmic-ray neutron sensing (CRNS) [Zreda *et al.*, 2008, 2012] has proven to be effective in serving representative data at relevant scales. The reported footprint radius of ≈ 300 m [Desilets and Zreda, 2013] is much larger than spatial correlation lengths of soil moisture patterns, typically ranging between 30 and 60 m [Western *et al.*, 2004]. Thereby, this technology outperforms conventional in-situ measurements in terms of representativeness for scales beyond several tens of meters.

Neutron radiation is omnipresent in the atmosphere as it is generated by a nearly constant incoming flux of cosmic rays. The presence of hydrogen near or in the ground reduces the neutron abundance in a predictable way. Especially the density of fast neutrons in air can serve as an efficient proxy for the quantity of ambient water. The continuous

monitoring of background radiation is a passive and non-invasive solution to the problem of representativeness, because the integral average over local water sources is an intrinsic property of the method.

Generally, spatial integration in the support volume of a measurement is intrinsic to most instruments in hydrogeophysics. When it comes to interpretation and validation, however, accurate knowledge of the spatial extent and sensitivity to environmental conditions is indispensable. For that reason, investigating an instrument's support volume is an active field of research in hydrogeophysics, e.g. considering time-domain reflectometry [Ferré *et al.*, 1996, 1998], ground-penetrating radar [see Huisman *et al.*, 2003, for a review] and nuclear magnetic resonance [Legchenko *et al.*, 2002; Lubczynski and Roy, 2004] among others. Methods based on the global positioning system [Larson *et al.*, 2008] or gravimetry [Creutzfeldt *et al.*, 2010; Kazama and Okubo, 2009] exhibit footprints comparable to the cosmic-ray neutron probe. However, the exact spatial sensitivity often remains unclear and thus limits the interpretation of measurements. In planetary space science, investigating an instrument's footprint is of fundamental importance, for instance, to improve the resolution and interpretation of gamma or neutron measurements [Lawrence *et al.*, 2003; Maurice *et al.*, 2004]. Monte Carlo simulations were consulted to inquire the geophysical support volume literally in depth [McKinney *et al.*, 2006].

Using neutron transport modeling based on the Monte Carlo method, footprint characteristics of the CRNS technique were presented initially by Zreda *et al.* [2008] and investigated in detail by Desilets and Zreda [2013] for idealized environmental conditions. The latter laid an important foundation to plan and improve sampling strategies and local site arrangement. According to Zreda *et al.* [2012], coastal transect experiments

confirmed the reported footprint radius of several hundreds of meters, but the detailed interpretation of these measurements appears to be challenging. Recent investigations with mobile neutron detectors suggest that the sensor responds to remote water bodies below the accepted theoretical distance. Furthermore, during the course of preliminary investigations the authors could observe an effect of extraordinary sensitivity to the very first meters around the sensor. Thus, doubts about the accepted exponential decrease are raised by measuring close to a shoreline or a small group of people, or comparing signals of many co-located sensors in a small patch. By using an alternative neutron source in the simulation, *Rosolem et al.* [2013] found that the detector is sensitive to water vapor in heights above the probe ranging from 412 m to 265 m for dry and wet air, respectively. Their results indicate that the assumptions on the modeled neutron source are decisive.

A more detailed understanding of the sensor's support volume becomes important as research projects expand to complicated terrain and mobile applications [e.g. *Dong et al.*, 2014]. An increasing number of CRNS probes are covering heterogeneous land which is often partly equipped with soil moisture monitoring networks [e.g. *Han et al.*, 2014; *Hawdon et al.*, 2014; *Zhu et al.*, 2015]. Previous studies focused on the applicability and evaluation of the CRNS method, where spatio-temporal conditions have mostly been homogenous [e.g. *Franz et al.*, 2012a]. Thereby it was difficult to identify invalid assumptions on the spatial sensitivity when point measurements were averaged. *Bogena et al.* [2013] identified this problem and applied a horizontally weighted average based on simulations from *Zreda et al.* [2008], but the authors did not compare it to the non-weighted average and so the open question remains whether this approach is advantageous. *Coopersmith et al.* [2014] introduced Voronoi-weights to differently vegetated parts of the footprint. However, the

distance to the cosmic-ray neutron sensor was not accounted for. In all these cases, a proper spatial weighting concept based on distance, depth and environmental conditions may lead to improved matching between the cosmic-ray derived soil moisture and the averaged validation data. Moreover, *Franz et al.* [2013b] show that large heterogeneous structures in the footprint can affect the average soil moisture signal apparent to sensors, because the neutron density and water content are non-linearly related [*Desilets et al.*, 2010]. This phenomenon again indicates that a proper spatial weighting of dry and wet spots could help to compensate for heterogeneity in the field.

To address the controversy about the footprint mentioned above as well as the needs for an accurate weighting function, we aim to minimize the number of physical simplifications in the numerical model. For example, many previous studies restrict simulations of neutron transport to very dry conditions in air or soil [e.g. *Zreda et al.*, 2012; *Franz et al.*, 2013b; *Zweck et al.*, 2013] and thus neglect the enormous influence of even small hydrogen sources to the fate of neutrons. Moreover, we are paying particular attention to a proper choice of the neutron source as model input.

In the past years various types of neutron source models have been chosen for particle transport simulations in order to study local effects of cosmic-ray neutron interactions. A common approach is to mimic incoming galactic cosmic rays by locating a neutron source at ≈ 8 km altitude and by sampling the neutron energies randomly from a primary cosmic-ray spectrum in a regime much above 100 MeV [e.g. *Franz et al.*, 2013b; *Rosolem et al.*, 2013; *Zweck et al.*, 2013]. On the other hand, *Desilets and Zreda* [2013] and *Shuttleworth et al.* [2013] applied an artificially distributed source below ground and sample from an evaporation spectrum that peaks at ≈ 1 MeV. This approach makes the consequential

assumption of a suppositional incoming cosmic-ray spectrum that is comprised of high-energy neutrons only. We will discuss both strategies in section 2.5. The short review shows that there is no clear agreement about proper energies and the location of the source. But as *Glasstone and Eddlund* [1952] and *Desilets and Zreda* [2013] argue, neutron transport is highly sensitive to the neutron’s initial energy.

Elaborated studies about atmospheric particle transport led to important progress in finding a reliable energy spectrum for cosmic-ray neutrons. *Sato and Niita* [2006] and *Sato et al.* [2008] simulated cosmic rays in the atmosphere covering a wide range of altitudes, cutoff-rigidities (roughly correlated to latitudes) and solar modulation potential. Analytical descriptions for neutron energy spectra are provided that have been validated with independent measurements. By choosing a parametrized energy spectrum of this kind, *Lifton et al.* [2014] recently resolved some long lasting discrepancies among scaling models for cosmogenic nuclide production.

In the same manner, we utilize the full available energy spectrum from *Sato and Niita* [2006] near the ground to refine previous neutron transport calculations. The objective of this study is to specify the footprint volume and radial sensitivity for various environmental conditions from arid to humid climate. We further investigate some of the open questions regarding the influence of topography, terrain, and water content in soil, air and vegetation.

2. Theory

Recognizing the complexity of environmental neutron physics is essential to interpreting observations and simulations. The neutron’s sensitivity to specific types of atoms can be high, but it further depends on neutron energy which in turn decreases with every

interaction [Rinard, 1991]. For instance, even small changes in the abundance of hydrogen can dramatically alter neutron interactions. Model simplifications, while necessary, should be introduced only with great care and their possible effects need to be assessed.

2.1. Primary Cosmic Rays

Cosmic radiation that is pounding the Earth originates mostly in our galaxy, e.g. from acceleration in shock regions of supernova remnants (see Blasi [2014] for a review). Protons are the main part of the particle flux, accompanied by other charged nuclei. The energy spectrum of the *primary cosmic rays* peaks at around 1 GeV per nucleon. Depending on their momentum, cosmic-ray particles may pass the geomagnetic fields of the Sun and the Earth. The solar magnetosphere leads to temporal variations of the cosmic-ray intensity based on the solar activity index. The planetary magnetosphere prevents cosmic rays from entering the atmosphere by deflecting particles below an energy-dependent cutoff rigidity r_c . Both effects further decrease the typical energies of incoming radiation to several hundreds of MeV per nucleon [e.g. Nesterenok, 2013; Grimani et al., 2011].

2.2. Neutron Generation in the Atmosphere

Secondary cosmic-ray particles (e.g., muons, protons, pions, neutrons) are generated by electromagnetic and nuclear interactions mostly in the outer part of the Earth's atmosphere. Their intensity peaks at the Pfofzer maximum (50–100 g/cm² atmospheric depth, Pfofzer [1936]) and decreases exponentially by several orders of magnitude towards sea level. However, altitudinal effects on the shape of the energy spectrum appear to be marginal [e.g. Nesterenok, 2013; Sato and Niita, 2006; Hands et al., 2009; Kowatari et al., 2005; Lei et al., 2005]. Typically, high-energy protons induce spallation of nitrogen or

oxygen nuclei in the atmosphere [e.g. *Letaw and Normand*, 1991]. This reaction releases a couple of neutrons which are in turn able to trigger further cascades. The physics of high-energy neutron interactions is not well-known and thus the attempt to describe the complete process is accompanied by uncertainty.

2.3. Energy Reduction by Air, Soil and Water

Above thermal energies, neutrons lose energy with every collision and cannot accelerate to higher energies due to their neutral electrical charge. The final energy spectrum for neutrons at ground level is depicted in Fig. 1, where three peaks are prominent. Highly energetic neutrons at ≈ 100 MeV (red) are produced by intra-nuclear cascades and pre-equilibrium processes [*Gudima et al.*, 1983]. When high-energy neutrons or protons interact with air or soil, the excited nuclei evaporate (i.e. release) the so-called *fast* neutrons at a lower energy. This process manifests itself at the peak at ≈ 1 MeV (green) and shows additional absorption fine structure due to distinct resonances of non-hydrogen atoms. Neutron interactions in the sub-MeV region (blue) are dominated by elastic collision, in which, as a rule of thumb, the energy loss is correlated to the mass of the target nucleus. Due to the extraordinarily low mass of hydrogen, this energy band is most sensitive to water and organic molecules and thus most relevant for the CRNS method. Below ≈ 1 eV the target is usually in thermal equilibrium with the environment. Here, the target's energy significantly contributes to the neutron's energy when transferred during a collision. As a consequence, neutrons finally become thermalized at $k_B T \approx 25$ meV (grey), where k_B is the Boltzmann constant. Since neutrons cannot leave the thermal equilibrium towards relevant energies, this work disclaims the lower part of the spectrum.

The probability of a neutron to interact with an atom is quantified by the term *cross section*. It exhibits large variations due to isotopic composition and atomic number. The atomic mass A classifies types of possible interactions. Very heavy nuclei with $A > 80$ like ^{235}U , can undergo fission and scatter fast neutrons inelastically. Intermediate nuclei of $25 < A < 80$ are able to absorb or scatter the neutron inelastically. Light nuclei with $A < 25$ predominantly perform elastic scattering of neutrons. The hydrogen nucleus, $A = 1$, exhibits exceptionally high absorption and elastic scattering cross sections. However, absorption is only significant in the thermal energy regime to which the ideal detector for measuring soil moisture is insensitive. Figure 2 shows neutron elastic scattering cross sections for elements that are most abundant in terrestrial air, water and solids. Water vapor, oxygen and nitrogen are particularly responsible for the neutron's deceleration in air. Therefore the range a neutron can travel before thermalization is expected to increase with altitude (i.e. decreasing air density) and decrease with increasing air humidity. On the other hand, dense soils, organic matter or soil water content are expected to reduce the penetration depth.

2.4. Spatial Mixing and its Analytical Description

Evaporated neutrons perform a random walk type of propagation, because the angular probability distribution of their interactions is mostly isotropic. In contrast, incoming high-energy neutrons do preferably interact in a forward directed process and thus vanish into the soil without reflection. In air, fast neutrons typically travel several tens of meters between collisions. And since hydrogen is most efficient in absorbing energy from the neutron, whereas air is less, information about remote water bodies can quickly propagate within hectometers. This process leads to a nearly homogeneous neutron density in the air

which can be sampled locally by the cosmic-ray neutron sensor and represents an average of ambient hydrogen abundance in soil, air and vegetation.

As a first order approach, one could expect neutrons to behave as a diffusive gas, as it was formulated by *Glasstone and Eddlund* [1952], and applied to a footprint estimate by *Desilets and Zreda* [2013] besides the modeling. But since every collision with a particle results in an energy loss for the neutrons, their mean free path between collisions changes and diffusion theory loses validity. The *Fermi age theory* [e.g. applied in *Barkov et al.*, 1957] accounts for these energy losses in a diffusive system, but analytical solutions exist only for mono-energetic particles and are not feasible for the cosmic-ray neutron spectrum exposed to a wide range of environmental atoms with different cross sections.

For these reasons, the assumption of homogeneous diffusion as applied by *Desilets and Zreda* [2013] will bias results toward neutrons with higher energies. Furthermore, the single-layer diffusion approach neglects the influence of the soil. Since neutrons interact with the soil and its water content on their path to the sensor, their energy is reduced more efficiently compared to the propagation in air. Therefore, the homogenous analytical approach overestimates the horizontal footprint radius and is rather valid for a vertical footprint above the surface. The phenomenon of exceptionally high vertical footprints was shown experimentally with a detector on a helicopter by M. Zreda (not published) and indirectly with numerical simulations [*Rosolem et al.*, 2013].

It is not feasible to join the complex problem of neutron transport, multi-energetic Fermi age theory and two-layer diffusion theory into a deterministic solution. Therefore statistical and numerical approaches are the only way to include all necessary factors involved.

2.5. In Quest of a Proper Model Input

Simulations of cosmic-ray neutrons near the ground require consolidated knowledge of the incoming radiation. However, the location of the source is commonly traded against computational effort, whereas the initial energy spectrum is bonded to a variety of uncertainties.

A popular approach is to launch secondary cosmic-ray neutrons at ≈ 8 km altitude and to perform their propagation through the atmosphere [e.g. *Franz et al.*, 2013b; *Rosolem et al.*, 2013; *Zweck et al.*, 2013]. This strategy and related simplifications come with several drawbacks:

1. Cross-sections of high-energy neutrons exhibit uncertainties of up to 50 % depending on element and type of reaction, though there has been progress in the last two decades [e.g. *Salvatores et al.*, 1994; *Palmiotti et al.*, 2007]. As a consequence, inconsistencies are apparent throughout different codes for galactic and atmospheric cosmic ray transport [e.g. *Lin et al.*, 2012; *Lei et al.*, 2005; *Sheu and Jiang*, 2003].

2. Measurements of cosmic-ray energy spectra are additionally accompanied by observational uncertainties. Comparative studies of Monte Carlo codes show differences of up to 20 % for calculating sensitivities of the neutron response to experimental devices [*Barros et al.*, 2014] and as well for the spectrum unfolding technique [*Rühm et al.*, 2014].

3. The exclusive neutron source at the top of the modeled atmosphere inadvertently neglects neutron generation throughout the atmosphere by other secondary particles like protons, pions and muons.

4. Atmospheric water vapor is often ignored, although hydrogen is the main moderator for neutrons.

5. The large difference in scale of the domain requires high computational effort to reach sufficient statistics.

Models which rely on particle propagation through the upper atmosphere incorporate a high complexity and vulnerability to such uncertainties involved.

In the attempt to reduce computational effort, other studies identified the high-energy component of the cosmic-ray neutron spectrum as the precursor for the generation of fast neutrons in the soil [Zreda *et al.*, 2008; Desilets and Zreda, 2013; Shuttleworth *et al.*, 2013]. Since the attenuation process of high-energy neutrons in the ground is known, it seems likely that an artificial source in the soil is sufficient to mimic the evaporative production of relevant neutrons. However, some drawbacks of this method are important to note:

1. Attenuation of high-energy neutrons in the soil follows an exponential decrease that is dependent on soil type and location on Earth [Gosse and Phillips, 2001].

2. There is no verified energy spectrum for neutrons in the soil. Evaporation neutrons are a significant part, but do not make up the spectrum as a whole (see Fig. 1).

3. In reality, the incoming energy spectrum from the atmosphere exhibits low-energy components and particularly neutrons which already evaporated in the air. On entering the soil, at least one interaction is needed to alter the direction back to the surface. In contrast, the artificially generated neutrons in the soil can escape without any interaction.

Considering only the evaporative neutrons in the soil can be a decent approach, especially for dry conditions. However, this strategy tends to overestimate average neutron energies, as incident low-energy neutrons from the top are neglected, and thus also overestimates the footprint size. Moreover, the deduced footprint appears to be insensitive to soil moisture, because its influence on neutron moderation is underestimated.

In this work, a different approach is applied, which aims to combine the advantages as well as avoid the drawbacks of both strategies mentioned above. To minimize the uncertainties of the propagated energy spectrum, this study focuses on the domain close to the surface by using validated results from independent atmospheric simulations as model input. This concept is computationally efficient and represents an established approach in planetary space science [e.g. *Tate et al.*, 2013].

Cosmic ray propagation in the atmosphere has been modeled thoroughly by *Sato and Niita* [2006]. They provide a reliable energy spectrum of cosmic-ray neutrons for a variety of altitudes, cutoff-rigidities, solar modulation potential and surface conditions. These simulations have been validated with various independent measurements at different altitudes and locations on Earth. Moreover, the analytical formulations of the spectra turned out to be effective in use for subsequent calculations. The presented energy-dependent flux $\phi(E)$ is described by a mean basic spectrum ϕ_B , a function for neutrons below 15 MeV ϕ_L , an extension for thermal neutrons (disclaimed in this work), and a modifier f_G for the geometry of the interface:

$$\phi(s, r_c, d, E, w) = \phi_B(s, r_c, d, E) \cdot f_G(E, w) \cdot \phi_L(s, r_c, d) ,$$

where w is the weight fraction of water in the ground. We focus our study on parameters for the atmospheric depth near sea level, $d = 1020 \text{ g/cm}^2$, solar maximum conditions $s = 1700 \text{ MV}$ and an exemplary cutoff rigidity of $r_c = 10 \text{ GV}$. This selection might introduce small differences for different places on Earth. However, *Goldhagen et al.* [2004] show that geomagnetic latitude has only very small effects on the shape of the spectrum. It depends slightly on atmospheric depth, as discussed by *Sato and Niita* [2006] and found by various

authors [e.g. *Sheu and Jiang*, 2003]. However, this is only significant for altitudes above several kilometers (see also section 2.2).

As such spectra generally consist of an incoming as well as a backscattered component, the appropriate incident spectrum was separated as follows. Firstly, for the given spectrum the response spectrum is calculated over pure water ($w = 1$), where the incoming component is dominant and thus the uncertainties of the calculation are minimal. Tracing the neutrons allows to determine an energy dependent multiplicity function $m(E)$ which allows to separate incoming ($m = 1$) from scattered parts ($m > 1$) of the spectrum. This filter can now be used to "subtract" only backscattered neutrons from the original spectrum. A thus recalculated spectrum contains only incident neutrons and can be used as the source of incoming radiation for any surface condition. It is provided in the supplementaries of this manuscript.

As an exception to the otherwise isotropic distribution, emission angles of high-energy neutrons above 10 MeV are highly collimated along the downward facing direction (nadir angle α). According to observations and simulations by *Nesterenok* [2013] the non-uniformity of the angular spectrum $J(\alpha)$ is given by:

$$J(\alpha) = e^{-2.4(1-\cos\alpha)} .$$

The presented strategy combines a universal and validated input spectrum and angular distribution for cosmic-ray neutrons with a reduced number of simplifications and a high computational efficiency.

2.6. Footprint Definition

The footprint of a geophysical instrument generally covers the area in which the medium of interest is probed and the carrier of such information is detected. The scenario of a centrally located sensor which detects neutrons isotropically exhibits point symmetry and thus leads to the assumption of a circular footprint area, $A = \pi r^2$. In this work we define the *travel distance* r as the Euclidean distance between the point of detection and the point of the neutron's first contact with the ground, also denoted as *origin*. Since r depends on the neutron's initial energy and number of collisions, it can range between 0–10³ m. Thus a quantile definition is needed to find a definite distance R within which most of the detected neutrons have probed the ground.

By assuming an exponential decay of detected neutron intensity over travel distance, which relates to the solution of a simple diffusion model, *Zreda et al.* [2008] and *Desilets and Zreda* [2013] legitimate the use of two e -folding lengths, i.e. the 86 % quantile, in order to define the footprint radius. Figure 3 illustrates the radial decrease of the detected neutron intensity W_r as a result of Monte Carlo simulations performed in this work. Although the calculated response does not exhibit a simple exponential shape, any other quantile would be an arbitrary choice as well. Careful interpretation of this value is recommended, however, because a high quantile value will always treat long-range neutrons with favour, regardless of how often they have probed the soil. Nevertheless, we decide to follow the definition of the 86 % quantile for historical reasons and denote the according footprint radius with R_{86} and the footprint area as $A = \pi R_{86}^2$.

The number of neutrons N_R that have originated within a distance R from the sensor is given by

$$N_R = \int_0^R W_r dr. \quad (1)$$

In order to find the distance within which 86% of the detected neutrons originate, the following equation is solved for R_{86} numerically:

$$\int_0^{R_{86}} W_r dr = 0.86 \int_0^\infty W_r dr. \quad (2)$$

In analogy we define the *penetration depth* D_{86} in the soil as the integral of a depth weighting function W_d which is expected to also decrease with distance r to the sensor.

3. Modeling

Monte Carlo simulations are able to track the histories of millions of neutrons. By taking all relevant physical interactions into account, the summary statistics of a large number of neutrons can reveal insights into their collective effects. In this study we apply the Monte Carlo method to address both large geometric scaling and anisotropic conditions.

3.1. Software

To address the specific needs of neutron-only interactions, we developed the Ultra Rapid Adaptable Neutron-Only Simulation (URANOS) based on the Monte Carlo approach for neutron transport. The software was originally developed to simulate specific characteristics of the Heidelberg neutron spin echo detectors and was adapted to the cosmic-ray neutron problem. The physics model follows the implementation declared by the ENDF database standard and described by OpenMC [*Romano and Forget, 2013*], a recent Monte Carlo code alternative to MCNP. It features the treatment of elastic collisions in the thermal, epithermal, and fast regime, as well as inelastic collisions, absorption and

absorption-like processes (e.g. evaporation) which play a dominant role for the given elements (these are the processes described by the ENDF MT identifiers 5, 103, 107, 208, 209, 210). Cross sections, energy distributions and angular distributions were taken from the databases ENDF/B-VII.1 [*Chadwick et al.*, 2011] and JENDL/HE-2007 [*Shibata et al.*, 2011].

The URANOS code was tailored to the problem of neutron transport in environmental science. By neglecting unnecessary physical processes (e.g. fission and gamma cascades) this leads to a significant increase in the computing speed compared to other available Monte Carlo codes for the description of neutron transport. In preparatory studies we explored the performance of the URANOS model in reproducing results from standard software like MCNPX. The tests successfully agreed in many different setups (not shown) such as the one presented by *Sato and Niita* [2006]. Particular attention was turned to the reproduction of the results from MCNPX performed by *Desilets and Zreda* [2013]. Using exactly the same setup of soil composition and source definition we were able to reproduce the reported footprint radius of ≈ 300 m and confirm the negligible dependence on soil moisture.

3.2. Neutron Source

Neutrons are launched from point sources randomly distributed in the region from 2 m to 42 m above the surface (Fig. 4). Energies are sampled from a pre-calculated spectrum based on *Sato and Niita* [2006], which is provided in the supplementaries of this manuscript. High-energy neutrons are launched with a collimated angular distribution (see section 2.5). The source intensity was chosen according to statistical errors. More

neutrons would lead to more accurate and smooth data. We experienced that 10^7 neutrons are a reasonable trade-off between computational effort and precision.

3.3. Detector

Neutrons are recorded individually in an horizontally infinite detector layer. Any neutron that experienced interaction with the soil is counted as it passes the layer. The infinite plane detector overlays the atmosphere by means of a 25 cm high sheet at a vertical position of 175–200 cm. This geometry was chosen because we aim to compare our results with *Desilets and Zreda* [2013], who tallied the neutron fluxes in a 2 m detector layer. The detector layer is crossed by the neutrons and thus maps the spatial field of neutron densities. It is an appropriate abstraction of a realistic, small-scale detector volume of the same height that absorbs neutrons. As tests confirm, multiple counts of a single neutron in the detector layer account for the measured density equivalent for a single count per volume detector. This relation holds if (1) the dimension of the absorbing detector medium stays below typical scale lengths of neutron interactions (10–100 m), and (2) particles do not scatter multiple times in that volume. That is very unlikely for non-thermal neutrons and furthermore does not factorize in the count statistics.

We refer to several statements of the effective energy range to which the detector is sensitive. Following practical considerations by *Desilets and Zreda* [2013] and theoretical by *Hertel and Davidson* [1985], the detection energy is set to a window from 10 eV to 10^3 eV. *Kouzes et al.* [2008] reports that the detection efficiency of moderated helium-3 detectors is nearly constant in that energy regime, which is why signal weighting for different energies is not needed.

Recent studies reported that the common cosmic-ray neutron detectors (presented by *Zreda et al.* [2012]) are contaminated by $\approx 30\%$ thermal neutrons [*McJannet et al.*, 2014]. We do not account for this issue, because this study aims to investigate characteristics for a detector ideally tailored to the needs of environmental water sensing.

3.4. Air, Soil and Water

The modeled pure air medium consists of 78 %_{Vol} nitrogen, 21 %_{Vol} oxygen and 1 %_{Vol} argon at a pressure of 1020 mbar. The soil extends to a depth of 6 m and the air to 1000 m. Both, soil and air are represented by planes of infinite extension, which can have subdomains, either to create a density profile in depth or to add specific entities like water or a detector. The soil consists of 50 %_{Vol} solids and a scalable amount of H₂O. The solid domain is comprised of 75 %_{Vol} SiO₂ and 25 %_{Vol} Al₂O₃ at a compound density of 2.86 g/cm³. Thus, the total densities vary from 1.43 g/cm³ to 1.93 g/cm³ for 0 %_{Vol} and 50 %_{Vol} soil moisture, respectively.

Further chemical constituents regarding rock types are not significant for fast neutron moderation, according to calculations from *Zreda et al.* [2012] and *Franz et al.* [2012b] and the discussion in section 2.3.

4. Results and Discussion

The response of the ground to the incoming flux of cosmic-ray neutrons lead to several interesting features in the resulting energy spectrum. Figure 5a,b confirms the efficient reduction of neutron intensity by soil moisture in the relevant energy range of the CRNS method. Figure 5c shows that water vapor particularly affects neutrons at the upper end of the energies considered. In this energy domain, neutrons cover the largest distances

and are consequently exposed to the highest path-integrated amount of air. In general, neutrons appear to be very sensitive to small amounts of hydrogen in soil and air.

4.1. Radial Footprint Changes with Humidity and Soil Moisture

We performed simulations with a variety of volumetric water contents in the soil from 0–50 % and absolute humidity in the air from 0–50 g/m³. Figure 3 illustrates the sensitivity of the detector to neutrons originating at different radial distances r . This *radial weighting function* W_r can assist in finding a properly weighted mean of independent soil moisture measurements. It further shows that little contribution is made by neutrons from $r > 200$ m and highest contribution comes from $r < 10$ m around the sensor.

The peak at $r < 10$ m accounts for neutrons that directly emerge from the ground and have a high probability to be detected even though most of them come from the lower part of the neutron energy spectrum. The region up to $r < 50$ m describes the average mean free path of most of the environmental neutrons in humid air. For distances between 50–200 m neutrons interact with the soil multiple times until they are detected, which in turn means that with increasing r , average neutron energies quickly become insufficient in order to arrive at the detector before thermalization. From about 200 m on, detected neutrons are dominated by the higher energetic part of the spectrum, which appear to be higher in flux rates and are able to probe the soil very far from the detector.

Due to the different neutron energies involved, we found an accurate fit to the intensity distribution (Fig. 3) by splitting the radial domain into four exponential parts. An analytical description can be obtained for $\theta \geq 2\%$:

$$W_r(h, \theta) \approx \begin{cases} F_1 e^{-F_2 r} + F_3 e^{-F_4 r}, & 0.5 \text{ m} < r \leq 50 \text{ m} \\ F_5 e^{-F_6 r} + F_7 e^{-F_8 r}, & 50 \text{ m} < r < 600 \text{ m} \end{cases} \quad (3)$$

where the parameter functions $F_i(h, \theta)$ are individually dependent on humidity and soil moisture as given in appendix A. The separation at $r = 50$ m accounts for the non-trivial shape of the function as described above. For $r > 50$ m both exponential terms describe diffusion-like processes each accounting for soil moisture and air humidity presence. On the contrary, in $r \leq 50$ m diffusion is not the main process, however, since the same functional structure still holds numerically, it was chosen for convenience. Following equation 2 we integrate $W_r(h, \theta)$ numerically. The resulting $R_{86}(h, \theta)$ is analytically difficult to grasp, thus we illustrate the numerically integrated results as contours in Figure 6 and present a numerical matrix in the supplementaries. The contour plot shows that the footprint radius ranges from 240 m to 130 m between arid and tropical climate, respectively.

The response to soil moisture variations is significant for humid climate between 10–40 %_{Vol} as well as for very dry conditions < 3 %_{Vol}. Previous studies underestimated the role of soil moisture for the footprint due to the choice of a modeled neutron source below the surface (see section 2.5). Comparative studies (not shown) indicated that this detail is the major cause for the discrepancy to findings from *Desilets and Zreda* [2013]. Moreover, the decrease of the footprint with increasing soil moisture does not necessarily imply that the area-average estimate is less representative. According to *Korres et al.* [2015], spatial variability of soil moisture tends to be low for rather wet soils. In this context, the effective representativeness of the CRNS method appears to be almost unchanged.

The response to variations of absolute humidity features a 10 m decrease of the footprint radius for every change of 4–6 g/m³ water vapor. *Zreda et al.* [2012] refers to ≈ 10 % reduction of the footprint from dry to saturated air, which can easily span ≈ 25 g/m³. This change corresponds to a 20 % change in footprint radius calculated with URANOS. How-

ever, *Desilets and Zreda* [2013] investigated the influence of humidity in further detail and found a 10 m decrease for every change of $\approx 6 \text{ g/m}^3$ humidity from MCNPX simulations with dry soil. This value is consistent with results from URANOS, whereas the slightly higher gradient is a consequence of the different energy spectra used in the models.

The function W_r lays the basis for a refinement of the commonly applied sampling strategy. The accepted method equally weights point measurements from three distinct radii [*Zreda et al.*, 2012; *Franz et al.*, 2012a] which correspond to an exponential weighting function (see section 2.4). In contrast, the present work shows that (1) the first tens of meters provide dominant contribution to the signal in a rather non-exponential relation, and (2) the shape of the weighting function changes temporally as it is affected by variable moisture conditions. It is therefore not possible to elaborate a universal sampling strategy. As a rule of thumb we recommend to take more samples closer to the probe (e.g. 0–10 m) than was previously recommended. Subsequently, data should be weighted with $W_r(h, \theta)$ in a post-processing mode (see appendix B).

4.2. Uncertainty Analysis

In the simulated system containing soil, atmosphere, and a detector, uncertainties propagate non-linearly due to the variety of neutron interactions involved. As an indication of their total effect, we analyzed uncertainties of our calculations by means of the influence on the footprint radius R_{86} .

Variations of cross sections by their standard deviation, given in the ENDF data base, lead to changes of R_{86} by 4 %, 3 %, and 2 % for $\theta = 3 \%$, 10 % and 40 %, respectively. The effect of elastic scattering dominates the budget by approximately 70 %. Further details about this analysis are provided in the supplementaries. The errors of the cross sections

can be considered as systematic for neutron transport simulations in general. We further analyzed the impact of different source spectra as model input in a test case with 10 % soil moisture and 5 g/m^3 air humidity. As explained in section 2.5 the incident spectrum was generated over water by subtracting the soil response from the original mixed spectrum. Variations of this soil response spectrum by 20 % alters R_{86} by 2.5 %. If the emission angles of source neutrons were not set according to their angular distributions, but chosen perpendicular to the surface, the change of the footprint radius would be 2.5 % applied to high energetic neutrons only and 3.0 % using sub-MeV neutrons. Compared to the uncertainties involved in our calculations the impact of other source spectrum models can be much higher. The integration of the counted particles (eq. 2) further leads to statistical uncertainties on R_{86} in the order of 0.2 % for 10^7 neutrons.

All in all we conservatively report a total error of $\Delta R_{86} = 4\text{--}6 \%$, which scales from wet to dry conditions.

4.3. Footprint Scaling with Vegetation and Air Pressure

To investigate the footprint variability under vegetated conditions, we modeled above-ground vegetation as a layer of height H_{veg} , containing an exemplary mixture of water and carbon with a density of $\rho_{\text{veg}} = 0.005 \text{ g/cm}^3$. This corresponds to $\approx 4.4 \text{ kg/m}^3$ biomass water equivalent (BWE), since we have chosen the molecular composition of the gas in a way that the living plant consists of $\approx 12 \%$ carbon by weight. For layer heights below a few meters, variations of either density or height have comparable effect on neutron moderation. Therefore, this method can provide valid estimations of the vegetation effect in terms of both, height and water equivalent.

From the perspective of the neutron, the layer introduces a new source of hydrogen in the air and consequently reduces the traveling range in the same manner as humidity. For example, the footprint radius is reduced by $\approx 20\%$ for crops of height $H_{\text{veg}} = 2\text{ m}$ ($\text{BWE} \approx 8.8\text{ kg/m}^2$) in dry soils. From simulations presented in Figure 7a we find an exponential dependence of the footprint scaling factor f_{veg} on vegetation height H_{veg} :

$$f_{\text{veg}}(\theta) = 1 - 0.17 \left(1 - e^{-0.41H_{\text{veg}}}\right) \left(1 + e^{-7\theta}\right), \quad (4)$$

where θ is given in units of m^3/m^3 . For thin vegetation cover a linearisation in H_{veg} is appropriate. As *Franz et al.* [2013c] demonstrate, water in above ground biomass influences the signal in another way than homogeneously distributed soil moisture, which is well reflected by the URANOS model approach (see also Fig. 5).

On the other hand, the footprint can also expand with decreasing air pressure (e.g. increasing altitude). The lower air density allows neutrons to cover longer distances between collisions. For example, the footprint can be 20% larger at a $\approx 2000\text{ m}$ altitude ($\simeq 800\text{ mbar}$) compared to sea level. Although a reciprocal fit is a reasonable estimate [*Desilets and Zreda*, 2013], our results presented in Figure 7b indicate an exponential dependence on p due to the presence of hydrogen:

$$f_p = \frac{0.5}{0.86 - e^{-p/p_0}} \approx p_0/p. \quad (5)$$

However, differences between the two models appear to be insignificant.

By taking the scaling factors into account, the final footprint radius can be estimated with

$$R_{86}(h, \theta, p, \text{veg}) = f_p \cdot f_{\text{veg}}(\theta) \cdot R_{86}(h, \theta). \quad (6)$$

An extreme case of vegetation is a forest site, where cosmic-ray sensors are placed to study the influence of wet biomass or interception water in the canopy [e.g. *Desilets et al.*, 2010]). In order to provide a first glimpse of the influence of a forest on the footprint, we set up a gas representing the molecular composition of an exemplary forest with a density of $\rho_{\text{forest}} = 0.0016 \text{ g/cm}^3$, which corresponds to $\approx 1.4 \text{ kg/m}^3$. Considering $h = 10 \text{ g/m}^3$ and $\theta = 10 \%$, our results indicate that the sensor footprint in a forested ecosystem is reduced to 78% or 44% for canopy heights of 15 m or 30 m, respectively. Qualitatively, this reduction should be taken into account when calibration or validation of the CRNS probe is performed in forests and in different seasons [e.g. *Franz et al.*, 2013a; *Bogena et al.*, 2013; *Lv et al.*, 2014]. Future investigations should focus on various vegetation models and cover a range of parameters in order to gain profound understanding of neutron interactions at individual agricultural or forest sites.

4.4. Penetration Depth in the Soil

The thickness of the probed soil layer is an important advantage of the CRNS method compared to most remote-sensing products. Cosmic-ray neutrons can penetrate the first decimeters of the soil almost unhindered, whereas electromagnetic signals interact within the upper 0–5 cm. *Franz et al.* [2012b] showed that the effective representation of the penetration depth, $z^*(\theta)$, is a reciprocal function of soil moisture, but it is unclear how it varies with the distance from the probe.

In URANOS we logged the vertical positions where neutrons lost energy in a scattering process, i.e. probed the soil. Above $\theta \geq 10 \%$, the penetration depth of neutrons appears to decrease exponentially. This behaviour can be expected from a simple mono-energetic Beer-Lambert approach [*Beer*, 1852], and has also been found by *Zreda et al.* [2008]. A

simple analytical description of the vertical weighting function was found for $\theta \geq 10\%$:

$$W_d(r, \theta) \propto e^{-2d/D_{86}(r, \theta)}. \quad (7)$$

The relation can be used to obtain a properly averaged mean value of point measurements when compared to the cosmic-ray derived estimates. The numerical determination of the penetration depth D_{86} , however, is certainly valid for any soil moisture condition $\theta \in (1..50\%)$:

$$D_{86}(r, \theta) = \rho_{\text{bd}}^{-1} \left(p_0 + p_1 \left(p_2 + e^{-r/100} \right) \frac{p_3 + \theta}{p_4 + \theta} \right). \quad (8)$$

The quantity denotes up to which depth 86% of the detected neutrons had contact with constituents of the soil. Numerical parameters are provided in Table A, θ is in units of m^3/m^3 .

Figure 8 shows penetration depths $D_{86}(r, \theta)$ as a function of radial distance r from the sensor for exemplary soil moisture values θ . For dry soil $D_{86}(r, \theta \approx 1\%)$ ranges from 83 cm right below the sensor to 46 cm at $r = 300$ m distance. At most, the penetration depth varies between 15 cm and 83 cm below the sensor for wet and dry soil, respectively. This is in close agreement with depths of 12–76 cm given by *Zreda et al.* [2008]. The reported values are rather confirmed than contradicted by URANOS, because they stemmed from experiences and various studies in the research field of cosmogenic nuclide production and are thus independent of the mentioned model approach. On average over the first tens of meters distance, the functional dependency on θ (eq. 8) is relatively similar to the reciprocal model for the *effective sensor depth* $z^*(\theta)$ from *Franz et al.* [2012b]. Their model was constrained on the limits introduced by *Zreda et al.* [2008] and validated with measurements and hydrodynamic simulations. Further evidence for the correct performance

of the URANOS model provides the comparison with measurement depths of 50 – 100 cm on the Moon or Mars missions, where cosmic-ray neutrons penetrate dry ground of similar chemical composition [Elphic *et al.*, 2008; McKinney *et al.*, 2006].

4.5. Terrain Structures and Topography

Cosmic-ray neutron probes are sometimes placed close to roads, trees, rivers or in hilly terrains. In an analogous manner mobile rover surveys inevitably pass alongside forests, lakes or fields of different land use. In most of these cases we do not expect an isotropic footprint of the probe, because large structures of different hydrogen content vary throughout the viewing directions.

In order to quantify the anisotropy of detected neutrons, we simulated four exemplary cases where such scenarios are extreme. In Figure 9 the vicinity of a centered detector is shown and the isotropic footprint $R_{86}(h = 5 \text{ g/m}^3, \theta = 5\%) = 210 \text{ m}$ is indicated (dashed line). Dots illustrate the origin of detected neutrons, where the closest 86% of total neutrons are emphasized (black) in each direction. We discretized the area into 12° sectors in order to quantify range (black dots) and intensity (red) for 30 discrete directions.

In a coast line setup (Fig. 9a) the density of the origins (dots) and neutron intensity (red) appear to be much smaller in the ponded area. The range of neutrons decreases by up to 30–40% although neutrons still manage to travel long distances over water. Their contribution to the count rate sharply drops to about 40% at the interface.

In Figure 9b the detector is placed 50 m away from a 10 m wide river. This setup can be found where cosmic-ray neutron probes are located within small catchments with creeks or irrigated land. Neutron origins clearly show that the river hardly contributes to the signal because most neutrons lose too much energy after probing water (see also point density

and neutron intensity for water, Fig. 9a). This is also visible in the intensity which shows a slight asymmetry towards the dry side. However, the setup reveals a slightly wider footprint in the direction to the river, as a consequence of the intensity gap.

A detector carried on a dry, concrete road (Fig. 9c) is a common scenario for rover applications [e.g. *Chrisman and Zreda*, 2013]. The sensor detects about 10–20% more neutrons per sector from the road than from other directions. However, the decrease of the footprint along the road due to short-range dominated contribution is marginal. The effect of the road is expected to be weaker for tarry material, as it contains hydrogen and carbon.

In Figure 9d we illustrate the investigation of neutron detection under more complex topography, here being a 20° steep hill slope. From detailed analysis we found that the uphill footprint (left) does not differ significantly from downhill (right), although small asymmetries in the neutron origins occur. Neutron intensity from uphill is about 0.26% higher compared to downhill, which is far beyond significance of the count rate.

These idealized cases demonstrate that the geometry of complex terrain only slightly influences soil moisture measurements with the cosmic-ray neutron sensor. However, the anisotropic contributions to the count rate should be investigated individually if accuracy matters. To add more reality to the scenarios, future studies on topography and structures should account for correlating quantities like gradients of air pressure, humidity, or soil moisture down the hill or close to rivers. As a consequence of more collisions and more efficient moderation, these quantities are expected to treat neutrons from uphill preferentially.

4.6. Experimental Evidence?

Since the footprint definition is based on a radial symmetry, direct empirical evidence is difficult to achieve with natural structures. However, approaching water surfaces and transiting the coast line has been a common procedure to determine the range of detected neutrons. For example, *Kuzhevskij et al.* [2003] moved the detector over a lake and interprets that the signal strength is hardly sensitive to neutrons from the land side at distances greater than 200 m. In the last years, many experiments with the COSMOS detector have been performed across a water-land boundary by the group of M. Zreda. First data from Oceanside Pier (California, US) indicate that the sensitive distance is on the order of 100–200 m at sea level.

With URANOS we made an attempt to reproduce these transect experiments by moving a 4 m square-shaped detector over pure water and land with exemplary soil moistures from 1 to 30 % and fixed air humidity $h = 10 \text{ g/m}^3$. Figure 10 illustrates the simulations and the two experiments mentioned above. Simulated signal strengths clearly correspond to the measurements and give an indication of the soil water content which was unknown at the time of the experiments. The signal gradient is asymmetric over water (left) and land (right), which agrees with results from [*Franz et al.*, 2013b], who investigated the influence of large wet structures on the signal strength. It is further interesting to note that R_{86} ranges from 168–220 m (according to the considered range in soil moisture, 1–30 %). However, these values cannot be identified in the experiment, because the signal is almost saturated by 150 m. Both effects can be explained by (1) the overestimation of dry over wet regions in the signal, as a consequence of the non-linear relation: $\theta \mapsto N$ [*Desilets et al.*, 2010], (2) the effective removal of traveling neutrons due to the presence

of a water body on their way to the detector, and (3) the non-radial geometry of the experiment.

We must conclude that transect experiments do not give a direct measure of the footprint radius under conditions where the instrument is usually applied. However, the presented data provide evidence for the valid performance of the URANOS model.

5. Summary and Conclusions

This work investigates the footprint defined as the water-sensitive support volume of the cosmic-ray neutron sensor. Previous simulations by *Desilets and Zreda* [2013] drew general conclusions from a number of model assumptions and provided a decent estimate of the footprint for dry conditions. The travel distance of neutrons probing the soil, however, is very sensitive to initial energies and even to small amounts of hydrogen on their way. As a consequence, the complexity of environmental neutron transport appears to impede any attempt to simplify the problem. Therefore, we felt the need for revisiting neutron transport models and for addressing some of the open questions regarding the radial sensitivity, humid climate, or terrain structures. Simulations in this work were performed by the Monte Carlo code URANOS, whereas the concept is applicable to any standard software. From the results of this work we draw the following conclusions:

1. The revised footprint radius $R_{86}(h, \theta, p, \text{veg})$ is 240 m (18 ha area) for bare soil and purely dry conditions at sea level. However, significant influence of soil moisture θ , humidity h and vegetation can further reduce the radius by more than 40 %. In contrast, decreasing air pressure may expand it by $\approx 1\%$ per 10 mbar. The total error ΔR_{86} was estimated conservatively to be about 4–6 %. The dynamic footprint has implications for

methods for the interpolation of survey data, irrigation management and data assimilation for hydrological models.

2. The signal strength per radial distance, $W_r(h, \theta)$, is highly non-linear in r , h and θ and exhibits extraordinary sensitivity to the first few meters. As a rule of thumb, at least half of the neutron intensity reflected by the soil is due to the first 50 m around the sensor. Consequently, dynamic weighting of horizontal averages can be essential for sensor calibration and validation with soil moisture monitoring networks.

3. The penetration depth $D_{86}(r, \theta)$ of detected neutrons directly below the sensor ranges from ≈ 15 to 83 cm depending on soil moisture. An exponential decrease with depth is a good estimate for the sensor's vertical sensitivity, whereas the depth in turn shrinks significantly with radial distance to the sensor.

4. The circular shape of the footprint remains isotropic for most field applications, like hilly terrain, nearby rivers or heterogeneous land. However, large water bodies or forests nearby can reduce range and intensity of detected neutrons from that direction. Dry roads can contribute to an overestimate of neutron counts by a few percent. While rover surveys are often exposed to a variety of environmental conditions, these findings can have implications for interpretation and geostatistical interpolation of spatial data.

5. Transect experiments can be helpful to investigate the detector response to remote water bodies. In the same manner they allow to validate input models and strategies for Monte Carlo driven simulations. URANOS is able to reproduce these measurements adequately, however, this method is not appropriate to give direct evidence for the radial footprint size.

The present study shows that the description of the footprint and neutron intensity is non-trivial to an exceptional degree. For this reason it is not possible to conclude with an easy and straight-forward analytical formulation. We recommend to read out values from the figures presented here or from numerical and highly resolved data given in the supplementaries. Individual simulations should be performed for every probe in order to analyze the local response specific to the surrounding environment.

Future work is needed to experimentally verify the results of this study. For example, to test the suggested spatial sensitivity of the sensors, the performance of weighted averages needs to be assessed for point data from sampling campaigns or soil moisture monitoring networks. Despite the dynamic characteristics of the footprint, the capability to average water content over a large volume is undisputed and remains a valuable advantage of the method of cosmic-ray neutron sensing in the field of soil moisture monitoring.

Appendix A: Parameter Functions

The parameter functions $F_i(h, \theta)$ in equation 3 have been obtained empirically. Units for air humidity h and soil moisture θ are g/m^3 and m^3/m^3 , respectively. Table A contains the related numerical parameters p_j . In the supplementaries we provide application-ready scripts to calculate W_r in R, MatLab and Excel.

$$F_1 = p_0 (1 + p_3 h) e^{-p_1 \theta} + p_2 (1 + p_5 h) - p_4 \theta,$$

$$F_2 = \left((p_4 h - p_0) e^{-\frac{p_1 \theta}{1 + p_5 \theta}} + p_2 \right) (1 + p_3 h),$$

$$F_3 = p_0 (1 + p_3 h) e^{-p_1 \theta} + p_2 - p_4 \theta,$$

$$F_4 = p_0 e^{-p_1 \theta} + p_2 - p_3 \theta + p_4 h,$$

$$F_5 = p_0 \left(0.02 - \frac{1}{p_5 (p_6 \theta + h - p_5)} \right)$$

$$\cdot (p_4 - \theta) e^{-p_1(\theta - p_4)} + p_2 (0.7 - h\theta p_3),$$

$$F_6 = p_0(h + p_1) + p_2\theta,$$

$$F_7 = \left(p_0 (1 - p_6 h) e^{-p_1\theta(1 - p_4 h)} + p_2 - p_5\theta \right) \cdot (2 + p_3 h),$$

$$F_8 = \left((p_4 h - p_0) e^{\frac{-p_1\theta}{1 + p_5 h + p_6\theta}} + p_2 \right) \cdot (2 + p_3 h).$$

Appendix B: Weighted Mean for Soil Moisture Comparisons

Equations 3 and 7 can be used to weight individual point measurements in order to validate or calibrate the signal apparent to a cosmic-ray neutron sensor.

The general procedure to obtain a weighted average $\langle \theta_k \rangle$ from measurements θ_k with the weighting function W_k is as follows:

$$\langle \theta_k \rangle = \frac{\sum_k \theta_k \cdot W_k}{\sum_k W_k}.$$

Let θ_{ij} be a sample of soil moisture at the depth d_j and distance r_i to the cosmic-ray neutron sensor. The field-mean soil moisture $\langle \theta_{ij} \rangle$ and humidity $\langle h \rangle$ can be averaged with the equal weight $W_{ij} = 1 \forall i, j$. We then suggest to firstly compute the vertical average $\langle \theta_j \rangle_i$ of the data at each point i with the weighting function $W_{d_j}(r_i, \langle \theta_{ij} \rangle)$, eq. 7. Secondly, these values can be averaged horizontally ($\forall i$) with the weighting function $W_{r_i}(\langle h \rangle, \langle \theta_{ij} \rangle)$, eq. 3.

Acknowledgments. Supporting animations are available online at <http://www.ufz.de/cosmosfootprint>. Supplementary information of this work include data for Fig. 6, scripts to calculate eq. 3, measurements from M. Zreda in Fig. 10, the incoming neutron source spectrum, and details of the uncertainty analysis for the cross sections. Data used to support figures 1, 2, and 10 can be found in the cited papers. URANOS was developed

for the project "Neutron Detectors for the MIEZE method" funded by the German Federal Ministry of Education and Research (BMBF), grant identifier: 05K10VHA. Source code and support for URANOS can be provided by M. Köhli. MS acknowledges kind support by the Helmholtz Impulse and Networking Fund through Helmholtz Interdisciplinary School for Environmental Research (HIGRADE). The contribution of MZ has been funded through the COSMOS project by the U.S. National Science Foundation, grant identifier: ATM-0838491. The present work benefited from stimulating and critical discussions with Darin Desilets (Hydroinnova LLC). MK thanks A. Nesterenok and T. Sato for fruitful discussions. MS thanks J. Mai, L. Schüler, J. Weimar, and U. Wollschläger for kind assistance and valuable comments. The research was funded and supported by Terrestrial Environmental Observatories (TERENO), which is a joint collaboration program involving several Helmholtz Research Centers in Germany.

References

- Barkov, L., V. Makarin, and K. Mukhin (1957), Measurement of the slowing down of neutrons in the energy range 1.46-0.025 eV in water, *Journal of Nuclear Energy (1954)*, 4(1), 94 – 102, doi:[http://dx.doi.org/10.1016/0891-3919\(57\)90124-9](http://dx.doi.org/10.1016/0891-3919(57)90124-9).
- Barros, S., V. Mares, R. Bedogni, M. Reginatto, A. Esposito, I. F. Goncalves, P. Vaz, and W. Rühm (2014), Comparison of unfolding codes for neutron spectrometry with Bonner spheres, *Radiation Protection Dosimetry*, 161(1-4), 46–52, doi:10.1093/rpd/nct353.
- Beer (1852), Bestimmung der Absorption des rothen Lichts in farbigen Flüssigkeiten, *Annalen der Physik*, 162(5), 78–88, doi:10.1002/andp.18521620505.
- Biswas, A. (2014), Season- and depth-dependent time stability for characterising representative monitoring locations of soil water storage in a hummocky landscape, *CATENA*,

116(0), 38 – 50, doi:<http://dx.doi.org/10.1016/j.catena.2013.12.008>.

Blasi, P. (2014), Recent results in cosmic ray physics and their interpretation, *Brazilian Journal of Physics*, 44(5), 426–440, doi:10.1007/s13538-014-0223-9.

Bogena, H. R., J. A. Huisman, R. Baatz, H.-J. Hendricks Franssen, and H. Vereecken (2013), Accuracy of the cosmic-ray soil water content probe in humid forest ecosystems: The worst case scenario, *Water Resources Research*, 49(9), 5778–5791, doi:10.1002/wrcr.20463.

Chadwick, M., M. Herman, P. Obloinsk, M. Dunn, Y. Danon, A. Kahler, D. Smith, B. Pritychenko, G. Arbanas, R. Arcilla, R. Brewer, D. Brown, R. Capote, A. Carlson, Y. Cho, H. Derrien, K. Guber, G. Hale, S. Hoblit, S. Holloway, T. Johnson, T. Kawano, B. Kiedrowski, H. Kim, S. Kunieda, N. Larson, L. Leal, J. Lestone, R. Little, E. McCutchan, R. MacFarlane, M. MacInnes, C. Mattoon, R. McKnight, S. Mughabghab, G. Nobre, G. Palmiotti, A. Palumbo, M. Pigni, V. Pronyaev, R. Sayer, A. Sonzogni, N. Summers, P. Talou, I. Thompson, A. Trkov, R. Vogt, S. van der Marck, A. Wallner, M. White, D. Wiarda, and P. Young (2011), ENDF/B-VII.1 nuclear data for science and technology: Cross sections, covariances, fission product yields and decay data, *Nuclear Data Sheets*, 112(12), 2887 – 2996, doi:<http://dx.doi.org/10.1016/j.nds.2011.11.002>, special Issue on ENDF/B-VII.1 Library.

Chrisman, B., and M. Zreda (2013), Quantifying mesoscale soil moisture with the cosmic-ray rover, *Hydrology and Earth System Sciences*, 17(12), 5097–5108, doi:10.5194/hess-17-5097-2013.

Coopersmith, E. J., M. H. Cosh, and C. S. Daughtry (2014), Field-scale moisture estimates using COSMOS sensors: A validation study with temporary networks and leaf-area-

- indices, *Journal of Hydrology*, 519, Part A(0), 637 – 643, doi:http://dx.doi.org/10.1016/j.jhydrol.2014.07.060.
- Creutzfeldt, B., A. Güntner, S. Vorogushyn, and B. Merz (2010), The benefits of gravimeter observations for modelling water storage changes at the field scale, *Hydrology and Earth System Sciences*, 14(9), 1715–1730, doi:10.5194/hess-14-1715-2010.
- Desilets, D., and M. Zreda (2013), Footprint diameter for a cosmic-ray soil moisture probe: Theory and Monte Carlo simulations, *Water Resources Research*, 49(6), 3566–3575, doi:10.1002/wrcr.20187.
- Desilets, D., M. Zreda, and T. Ferré (2010), Nature’s neutron probe: Land surface hydrology at an elusive scale with cosmic rays, *Water Resources Research*, 46(11), doi:10.1029/2009WR008726.
- Dong, J., T. E. Ochsner, M. Zreda, M. H. Cosh, and C. B. Zou (2014), Calibration and validation of the cosmos rover for surface soil moisture measurement, *Vadose Zone Journal*, 13(4), –, doi:doi:10.2136/vzj2013.08.0148.
- Elphic, R. C., P. Chu, S. Hahn, M. R. James, D. J. Lawrence, T. H. Prettyman, J. B. Johnson, and R. K. Podgorney (2008), Surface and downhole prospecting tools for planetary exploration: tests of neutron and gamma ray probes, *Astrobiology*, 8(3), 639–52.
- Ferré, P. A., D. L. Rudolph, and R. G. Kachanoski (1996), Spatial averaging of water content by time domain reflectometry: Implications for twin rod probes with and without dielectric coatings, *Water Resources Research*, 32(2), 271–279, doi:10.1029/95WR02576.

- Ferré, P. A., J. H. Knight, D. L. Rudolph, and R. G. Kachanoski (1998), The sample areas of conventional and alternative time domain reflectometry probes, *Water Resources Research*, *34*(11), 2971–2979, doi:10.1029/98WR02093.
- Franz, T., M. Zreda, R. Rosolem, B. K. Hornbuckle, S. L. Irvin, H. Adams, T. E. Kolb, C. Zweck, and W. J. Shuttleworth (2013a), Ecosystem-scale measurements of biomass water using cosmic ray neutrons, *Geophysical Research Letters*, *40*(1936), doi:10.1002/grl.50791.
- Franz, T. E., M. Zreda, R. Rosolem, and T. Ferré (2012a), Field Validation of a Cosmic-Ray Neutron Sensor Using a Distributed Sensor Network, *Vadose Zone Journal*, *11*(4), doi:10.2136/vzj2012.0046.
- Franz, T. E., M. Zreda, T. P. A. Ferré, R. Rosolem, C. Zweck, S. Stillman, X. Zeng, and W. J. Shuttleworth (2012b), Measurement depth of the cosmic ray soil moisture probe affected by hydrogen from various sources, *Water Resources Research*, *48*(8), doi:10.1029/2012WR011871.
- Franz, T. E., M. Zreda, T. P. A. Ferré, and R. Rosolem (2013b), An assessment of the effect of horizontal soil moisture heterogeneity on the area-average measurement of cosmic-ray neutrons, *Water Resources Research*, *49*(10), 6450–6458, doi:10.1002/wrcr.20530.
- Franz, T. E., M. Zreda, R. Rosolem, and T. P. A. Ferré (2013c), A universal calibration function for determination of soil moisture with cosmic-ray neutrons, *Hydrology and Earth System Sciences*, *17*(2), 453–460, doi:10.5194/hess-17-453-2013.
- Glasstone, S., and M. C. Edlund (1952), *The elements of nuclear reactor theory.*, vii, 416 p. pp., Van Nostrand, New York, includes index.

- Goldhagen, P., M. Reginatto, T. Kniss, J. Wilson, R. Singleterry, I. Jones, and W. V. Steveninck (2002), Measurement of the energy spectrum of cosmic-ray induced neutrons aboard an ER-2 high-altitude airplane, *Nuclear Instruments and Methods in Physics Research Section A: Accelerators, Spectrometers, Detectors and Associated Equipment*, 476(12), 42 – 51, doi:[http://dx.doi.org/10.1016/S0168-9002\(01\)01386-9](http://dx.doi.org/10.1016/S0168-9002(01)01386-9).
- Goldhagen, P., J. Clem, and J. Wilson (2004), The energy spectrum of cosmic-ray induced neutrons measured on an airplane over a wide range of altitude and latitude, *Radiation Protection Dosimetry*, 110(1-4), 387–392, doi:10.1093/rpd/nch216.
- Gosse, J. C., and F. M. Phillips (2001), Terrestrial in situ cosmogenic nuclides: theory and application, *Quaternary Science Reviews*, 20(14), 1475 – 1560, doi:[http://dx.doi.org/10.1016/S0277-3791\(00\)00171-2](http://dx.doi.org/10.1016/S0277-3791(00)00171-2).
- Grimani, C., H. M. Arajo, M. Fabi, A. Lobo, I. Mateos, D. N. A. Shaul, T. J. Sumner, and P. Wass (2011), Galactic cosmic-ray energy spectra and expected solar events at the time of future space missions, *Classical and Quantum Gravity*, 28(9), 094,005.
- Gudima, K., S. Mashnik, and V. Toneev (1983), Cascade-exciton model of nuclear reactions, *Nuclear Physics A*, 401(2), 329 – 361, doi:[http://dx.doi.org/10.1016/0375-9474\(83\)90532-8](http://dx.doi.org/10.1016/0375-9474(83)90532-8).
- Han, X., R. Jin, X. Li, and S. Wang (2014), Soil moisture estimation using cosmic-ray soil moisture sensing at heterogeneous farmland, *Geoscience and Remote Sensing Letters, IEEE*, 11(9), 1659–1663, doi:10.1109/LGRS.2014.2314535.
- Hands, A., C. S. Dyer, and F. Lei (2009), SEU Rates in Atmospheric Environments: Variations Due to Cross-Section Fits and Environment Models, *IEEE Transactions on Nuclear Science*, 56, 2026–2034, doi:10.1109/TNS.2009.2013466.

- Hawdon, A., D. McJannet, and J. Wallace (2014), Calibration and correction procedures for cosmic-ray neutron soil moisture probes located across Australia, *Water Resources Research*, *50*(6), 5029–5043, doi:10.1002/2013WR015138.
- Hertel, N. E., and J. W. Davidson (1985), The response of Bonner spheres to neutrons from thermal energies to 17.3 MeV, *Nuclear Instruments and Methods in Physics Research A*, *238*, 509–516, doi:10.1016/0168-9002(85)90494-2.
- Huisman, J. A., S. S. Hubbard, J. D. Redman, and A. P. Annan (2003), Measuring soil water content with ground penetrating radar: A review, *Vadose Zone Journal*, *2*(4), 476–491, doi:10.2113/2.4.476.
- Kazama, T., and S. Okubo (2009), Hydrological modeling of groundwater disturbances to observed gravity: Theory and application to asama volcano, central japan, *Journal of Geophysical Research: Solid Earth*, *114*(B8), doi:10.1029/2009JB006391.
- Korres, W., T. Reichenau, P. Fiener, C. Koyama, H. Bogena, T. Cornelissen, R. Baatz, M. Herbst, B. Diekkirger, H. Vereecken, and K. Schneider (2015), Spatio-temporal soil moisture patterns a meta-analysis using plot to catchment scale data, *Journal of Hydrology*, *520*(0), 326 – 341, doi:http://dx.doi.org/10.1016/j.jhydrol.2014.11.042.
- Kouzes, R. T., E. R. Siciliano, J. H. Ely, P. E. Keller, and R. J. McConn (2008), Passive neutron detection for interdiction of nuclear material at borders, *Nuclear Instruments and Methods in Physics Research Section A: Accelerators, Spectrometers, Detectors and Associated Equipment*, *584*(23), 383 – 400, doi:http://dx.doi.org/10.1016/j.nima.2007.10.026.
- Kowatari, M., K. Nagaoka, S. Satoh, Y. Ohta, J. Abukawa, S. Tachimori, and T. Nakamura (2005), Evaluation of the altitude variation of the cosmic-ray induced environ-

- mental neutrons in the mt. fuji area, *Journal of Nuclear Science and Technology*, 42(6), 495–502, doi:10.1080/18811248.2004.9726416.
- Kuzhevskij, B., O. Y. Nechaev, E. Sigaeva, and V. Zakharov (2003), Neutron flux variations near the earth’s crust. a possible tectonic activity detection, *Natural Hazards and Earth System Science*, 3(6), 637–645, doi:10.5194/nhess-3-637-2003.
- Larson, K. M., E. E. Small, E. D. Gutmann, A. L. Bilich, J. J. Braun, and V. U. Zavorotny (2008), Use of GPS receivers as a soil moisture network for water cycle studies, *Geophysical Research Letters*, 35(24), n/a–n/a, doi:10.1029/2008GL036013.
- Lawrence, D. J., R. C. Elphic, W. C. Feldman, T. H. Prettyman, O. Gasnault, and S. Maurice (2003), Small-area Thorium features on the lunar surface, *Journal of Geophysical Research: Planets*, 108(E9), doi:10.1029/2003JE002050.
- Legchenko, A., J.-M. Baltassat, A. Beauce, and J. Bernard (2002), Nuclear magnetic resonance as a geophysical tool for hydrogeologists, *Journal of Applied Geophysics*, 50(12), 21 – 46, doi:http://dx.doi.org/10.1016/S0926-9851(02)00128-3.
- Lei, F., A. Hands, S. Clucas, C. Dyer, and P. Truscott (2005), Improvements to and validations of the QinetiQ atmospheric radiation model (qarm), in *Radiation and Its Effects on Components and Systems, 2005. RADECS 2005. 8th European Conference on*, pp. D3–1–D3–8, doi:10.1109/RADECS.2005.4365581.
- Letaw, J. R., and E. Normand (1991), Guidelines for predicting single-event upsets in neutron environments, *Nuclear Science, IEEE Transactions on*, 38(6), 1500–1506, doi:10.1109/23.124138.
- Lifton, N., T. Sato, and T. J. Dunai (2014), Scaling in situ cosmogenic nuclide production rates using analytical approximations to atmospheric cosmic-ray fluxes, *Earth and*

Planetary Science Letters, 386(0), 149 – 160, doi:http://dx.doi.org/10.1016/j.epsl.2013.10.052.

Lin, Z., J. A. Jr., A. Barghouty, S. Randeniya, R. Tripathi, J. Watts, and P. Yepes (2012), Comparisons of several transport models in their predictions in typical space radiation environments, *Advances in Space Research*, 49(4), 797 – 806, doi:http://dx.doi.org/10.1016/j.asr.2011.11.025.

Lubczynski, M., and J. Roy (2004), Magnetic resonance sounding: New method for ground water assessment, *Ground Water*, 42(2), 291–309, doi:10.1111/j.1745-6584.2004.tb02675.x.

Lv, L., T. E. Franz, D. A. Robinson, and S. B. Jones (2014), Measured and modeled soil moisture compared with cosmic-ray neutron probe estimates in a mixed forest, *Vadose Zone Journal*, 13(12), –.

Maurice, S., D. J. Lawrence, W. C. Feldman, R. C. Elphic, and O. Gasnault (2004), Reduction of neutron data from lunar prospector, *Journal of Geophysical Research: Planets*, 109(E7), doi:10.1029/2003JE002208.

McJannet, D., T. Franz, A. Hawdon, D. Boadle, B. Baker, A. Almeida, R. Silberstein, T. Lambert, and D. Desilets (2014), Field testing of the universal calibration function for determination of soil moisture with cosmic-ray neutrons, *Water Resources Research*, 50(6), 5235–5248, doi:10.1002/2014WR015513.

McKinney, G. W., D. J. Lawrence, T. H. Prettyman, R. C. Elphic, W. C. Feldman, and J. J. Hagerty (2006), MCNPX benchmark for cosmic ray interactions with the Moon, *Journal of Geophysical Research: Planets*, 111(E6), doi:10.1029/2005JE002551.

- Nesterenok, A. (2013), Numerical calculations of cosmic ray cascade in the Earth's atmosphere - Results for nucleon spectra, *Nuclear Instruments and Methods in Physics Research B*, 295, 99–106, doi:10.1016/j.nimb.2012.11.005.
- Palmiotti, G., M. Salvatores, G. Aliberti, Nuclear Engineering Division, and CEA Cadarache (2007), Validation of simulation codes for future systems: motivations, approach, and the role of nuclear data, in *Proceedings of the Fourth Workshop on Neutron Measurements, Evaluations and Applications*, INL.
- Pfotzer, G. (1936), Dreifachkoinzidenzen der Ultrastrahlung aus vertikaler Richtung in der Stratosphäre, *Zeitschrift für Physik*, 102(1-2), 41–58, doi:10.1007/BF01336830.
- Rinard, P. (1991), Neutron interactions with matter, *Passive Non-destructive Assay of Nuclear Materials.*, pp. 357–377.
- Romano, P., and B. Forget (2013), The OpenMC Monte Carlo particle transport code, *Annals of Nuclear Energy*, 51(0), 274 – 281, doi:http://dx.doi.org/10.1016/j.anucene.2012.06.040.
- Rosolem, R., W. J. Shuttleworth, M. Zreda, T. E. Franz, X. Zeng, and S. a. Kurc (2013), The Effect of Atmospheric Water Vapor on Neutron Count in the Cosmic-Ray Soil Moisture Observing System, *Journal of Hydrometeorology*, 14(5), 1659–1671, doi:10.1175/JHM-D-12-0120.1.
- Rühm, W., V. Mares, C. Pioch, S. Agosteo, A. Endo, M. Ferrarini, I. Rakhno, S. Rollet, D. Satoh, and H. Vincke (2014), Comparison of Bonner sphere responses calculated by different Monte Carlo codes at energies between 1 MeV and 1 GeV - potential impact on neutron dosimetry at energies higher than 20 MeV, *Radiation Measurements*, 67(0), 24 – 34, doi:http://dx.doi.org/10.1016/j.radmeas.2014.05.006.

- Salvatores, M., Nuclear Energy Agency, and Organisation for Economic Co-Operation and Development (1994), A first approach to data needs and target accuracies for hybrid systems, in *Intermediate Energy Nuclear Data: Models and Codes*, vol. 27, pp. 313–324.
- Sato, T., and K. Niita (2006), Analytical functions to predict cosmic-ray neutron spectra in the atmosphere, *Radiation Research*, 166(3), 544–555, doi:10.1667/RR0610.1.
- Sato, T., H. Yasuda, K. Niita, A. Endo, and L. Sihver (2008), Development of parma: Phits-based analytical radiation model in the atmosphere, *Radiation Research*, 170(2), 244–259.
- Sheu, R., and S. Jiang (2003), Cosmic-ray-induced neutron spectra and effective dose rates near air/ground and air/water interfaces in Taiwan, *Health Physics*, 84(1), 92–99, doi:10.1097/00004032-200301000-00008.
- Shibata, K., O. Iwamoto, T. Nakagawa, N. Iwamoto, A. Ichihara, S. Kunieda, S. Chiba, K. Furutaka, N. Otuka, T. Ohsawa, T. Murata, H. Matsunobu, A. Zukeran, S. Kamada, and J. Katakura (2011), JENDL-4.0: A new library for nuclear science and engineering, *Journal of Nuclear Science and Technology*, 48(1), 1–30, doi:10.1080/18811248.2011.9711675.
- Shuttleworth, J., R. Rosolem, M. Zreda, and T. Franz (2013), The cosmic-ray soil moisture interaction code (COSMIC) for use in data assimilation, *Hydrology and Earth System Sciences*, 17(8), 3205–3217, doi:10.5194/hess-17-3205-2013.
- Tate, C., J. Moersch, I. Jun, C. Hardgrove, M. Mischna, M. Litvak, A. Varenikov, I. Mitrofanov, A. Behar, W. Boynton, L. Deflores, F. Fedosov, D. Golovin, K. Harshman, A. Kozyrev, A. Malakhov, R. Milliken, M. Mokrousov, S. Nikiforov, A. Sanin, A. Vostrukhin, and MSL Science Team (2013), Diurnal variations in MSL DAN pas-

- sive measurements with atmospheric pressure and soil temperature, *44th Lunar and Planetary Science Conference*, p. 1601.
- Vereecken, H., R. Kasteel, J. Vanderborght, and J. Harter (2007), Upscaling Hydraulic Properties and Soil Water Flow Processes in Heterogeneous Soils: A Review, *Vadose zone journal*, *6*, 1 – 28, doi:10.2136/vzj2006.0055, record converted from VDB: 12.11.2012.
- Vereecken, H., J. A. Huisman, H. Bogaen, J. Vanderborght, J. A. Vrugt, and J. W. Hopmans (2008), On the value of soil moisture measurements in vadose zone hydrology: A review, *Water Resources Research*, *44*(4), n/a–n/a, doi:10.1029/2008WR006829.
- Wagner, W., G. Blöschl, P. Pampaloni, J.-C. Calvet, B. Bizzarri, J.-P. Wigneron, and Y. Kerr (2007), Operational readiness of microwave remote sensing of soil moisture for hydrologic applications, *Nordic Hydrology*, *38*(1), 1–20.
- Western, A. W., S.-L. Zhou, R. B. Grayson, T. A. McMahon, G. Blöschl, and D. J. Wilson (2004), Spatial correlation of soil moisture in small catchments and its relationship to dominant spatial hydrological processes, *Journal of Hydrology*, *286*(14), 113 – 134, doi:http://dx.doi.org/10.1016/j.jhydrol.2003.09.014.
- Zhu, Z., L. Tan, S. Gao, and Q. Jiao (2015), Observation on soil moisture of irrigation cropland by cosmic-ray probe, *Geoscience and Remote Sensing Letters, IEEE*, *12*(3), 472–476, doi:10.1109/LGRS.2014.2346784.
- Zreda, M., D. Desilets, T. P. A. Ferré, and R. L. Scott (2008), Measuring soil moisture content non-invasively at intermediate spatial scale using cosmic-ray neutrons, *Geophysical Research Letters*, *35*(21), doi:10.1029/2008GL035655.

Zreda, M., W. J. Shuttleworth, X. Zeng, C. Zweck, D. Desilets, T. Franz, and R. Rosolem (2012), COSMOS: The COsmic-ray Soil Moisture Observing System, *Hydrology and Earth System Sciences*, 16(11), 4079–4099, doi:10.5194/hess-16-4079-2012.

Zweck, C., M. Zreda, and D. Desilets (2013), Snow shielding factors for cosmogenic nuclide dating inferred from Monte Carlo neutron transport simulations, *Earth and Planetary Science Letters*, 379(0), 64 – 71, doi:http://dx.doi.org/10.1016/j.epsl.2013.07.023.

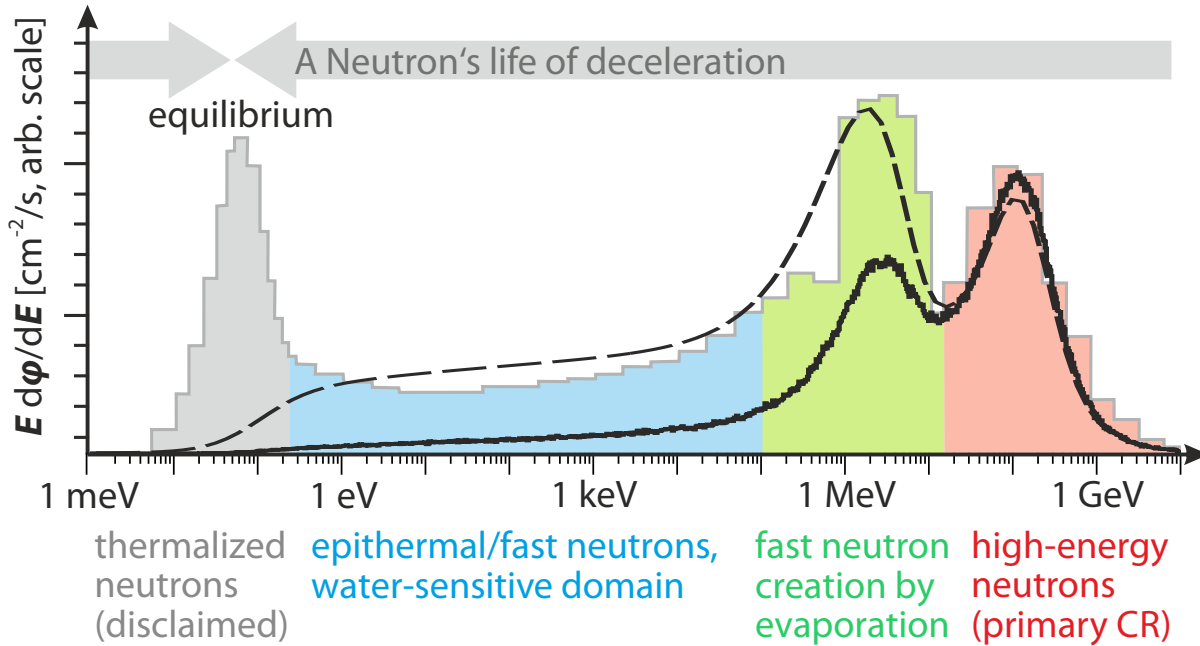


Figure 1. Neutron energy spectra at the surface: exemplary measurement by *Goldhagen et al.* [2002] (grey) and simulated by *Sato and Niita* [2006] (dashed). After subtracting the ground reflected component over pure water, we obtain a pure incoming component (continuous black line) which is used as the source spectrum in this study. Colors illustrate the deceleration of initial high-energy neutrons (red) which interact with heavy atoms leading to the evaporation spectrum (green). Energy is lost by elastic collisions with light atoms in the regime where the detector is particularly sensitive (blue) until neutrons arrive energetically in a thermal equilibrium (light grey).

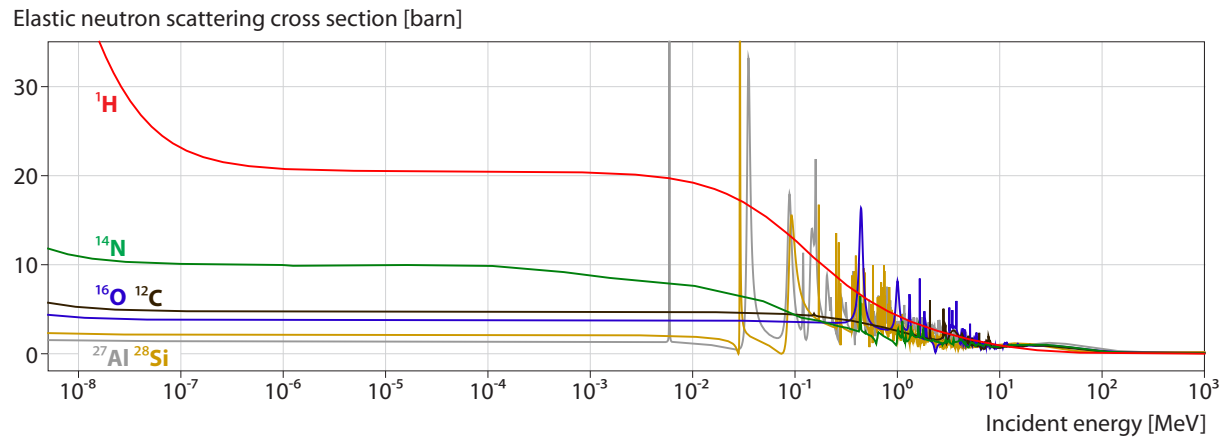


Figure 2. Comparison of elastic neutron cross sections of hydrogen (red), nitrogen (green), oxygen (blue), carbon (black), silicon (ocher), and aluminum (grey) for kinetic energies between 5 meV and 1000 MeV, data taken from JENDL/HE-2007 [Shibata *et al.*, 2011].

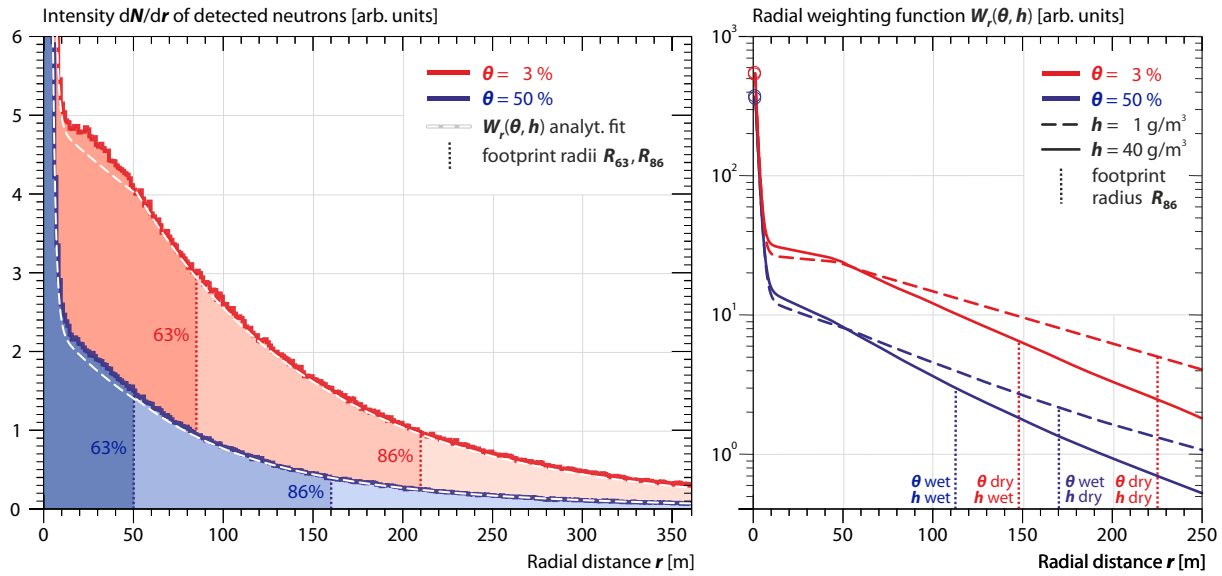


Figure 3. Detected neutron intensity dN/dr over distance r between origin and detection. The analytical fit is also called *radial weighting function* W_r . (Left): Simulations were performed for humidity $h = 10 \text{ g/m}^3$ and two exemplary soil moistures $\theta = 3\%$ and 50% . Quantiles declare footprint radii R_{63} and R_{86} (dotted) for $1 - e^{-1} \approx 63\%$ and $1 - e^{-2} \approx 86\%$ cumulative counts, respectively. Peaks at $r < 10 \text{ m}$ reach 57.5 for $\theta = 3\%$ and 37.9 for $\theta = 50\%$ according to the chosen scale. (Right): Comparison of W_r and the corresponding R_{86} for four extreme cases of soil moisture and humidity. Both quantities are shaping the curves differently.

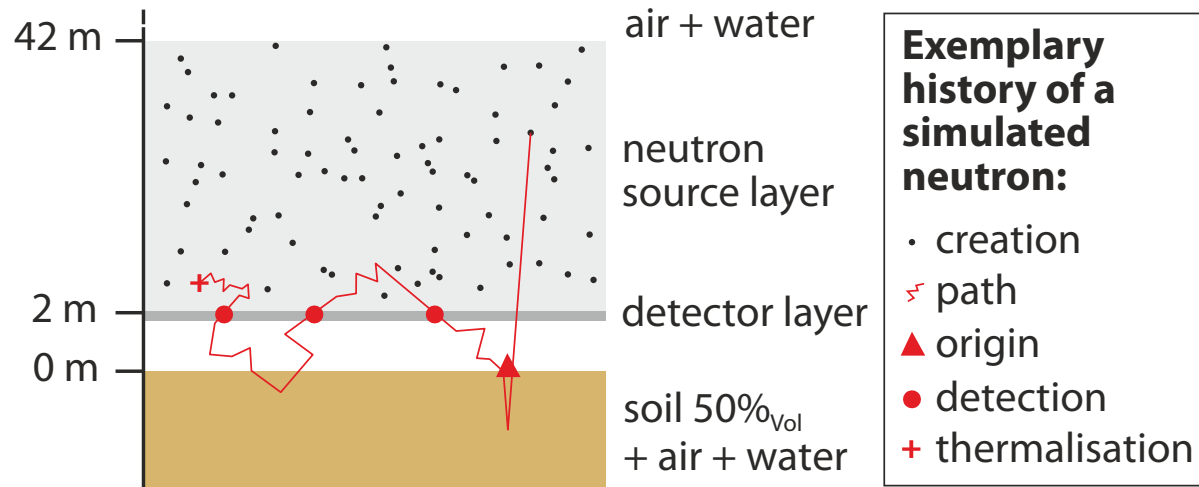


Figure 4. Setup of the simulation containing a 40 m thick neutron source layer in the atmosphere and a thin detector layer at 2 m above ground. A passing neutron is counted if it had preceding contact with the soil. The footprint is determined based on the distance between the origin and detection.

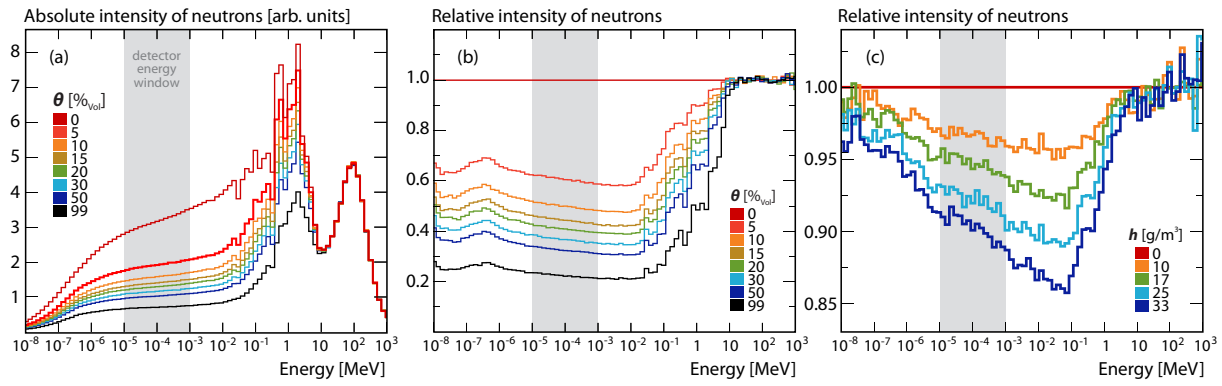


Figure 5. Calculated neutron spectra above ground with the highlighted energy window of the detector (grey) and the disclaimed thermal domain to its left, (a) for different soil moistures at an air humidity of 10 g/m^3 , (b) intensities of (a) scaled relative to 0% volumetric soil moisture, (c) intensities for different air humidities relative to 0 g/m^3 at 10% volumetric soil moisture.

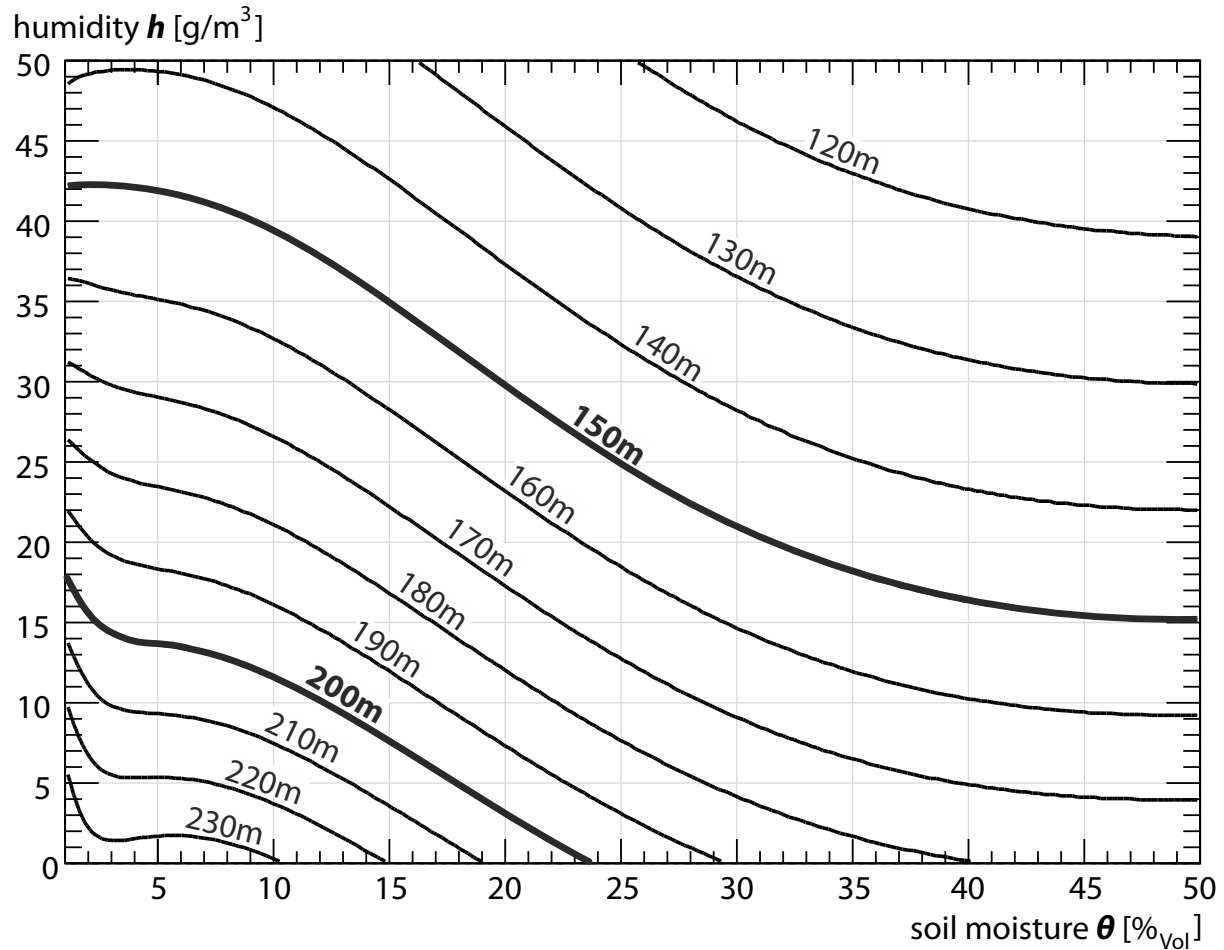


Figure 6. Footprint radius R_{86} (contour lines) and its dependency on soil moisture θ and air humidity h at sea level calculated by eqs. 2 and 3. Complex response to small amounts of hydrogen is evident. Corresponding data is provided in the supplementaries.

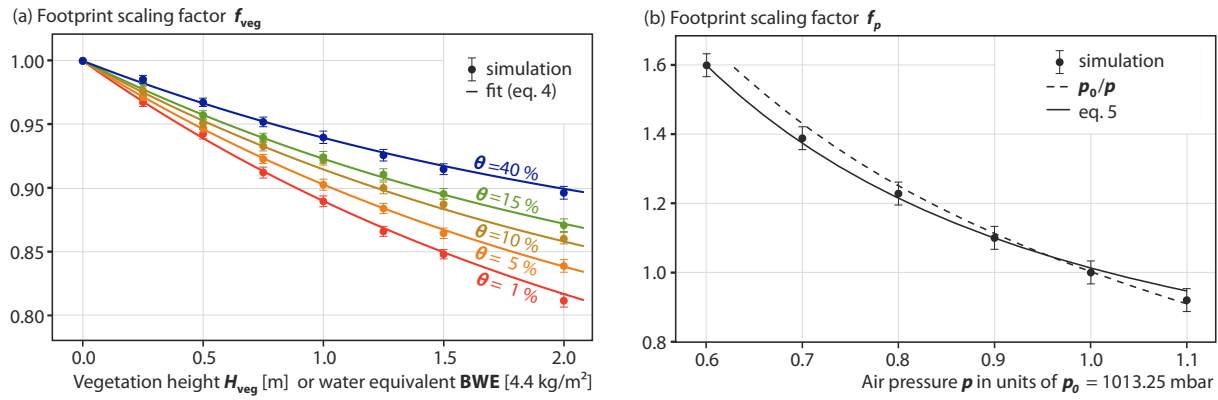


Figure 7. Change of the footprint radius $R_{86}(h, \theta)$ by vegetation and air pressure. (a): The scaling factor f_{veg} is reduced by vegetation height which corresponds to a biomass water equivalent. The effect is weakened by increasing soil moisture and air humidity, the latter was fixed to $h = 10 \text{ g/m}^3$ in this example. (b): The scaling factor f_p increases with altitude, which corresponds to decreasing air pressure. In this simulation we consider $h = 5 \text{ g/m}^3 \forall p$ and $\theta = 5 \%$.

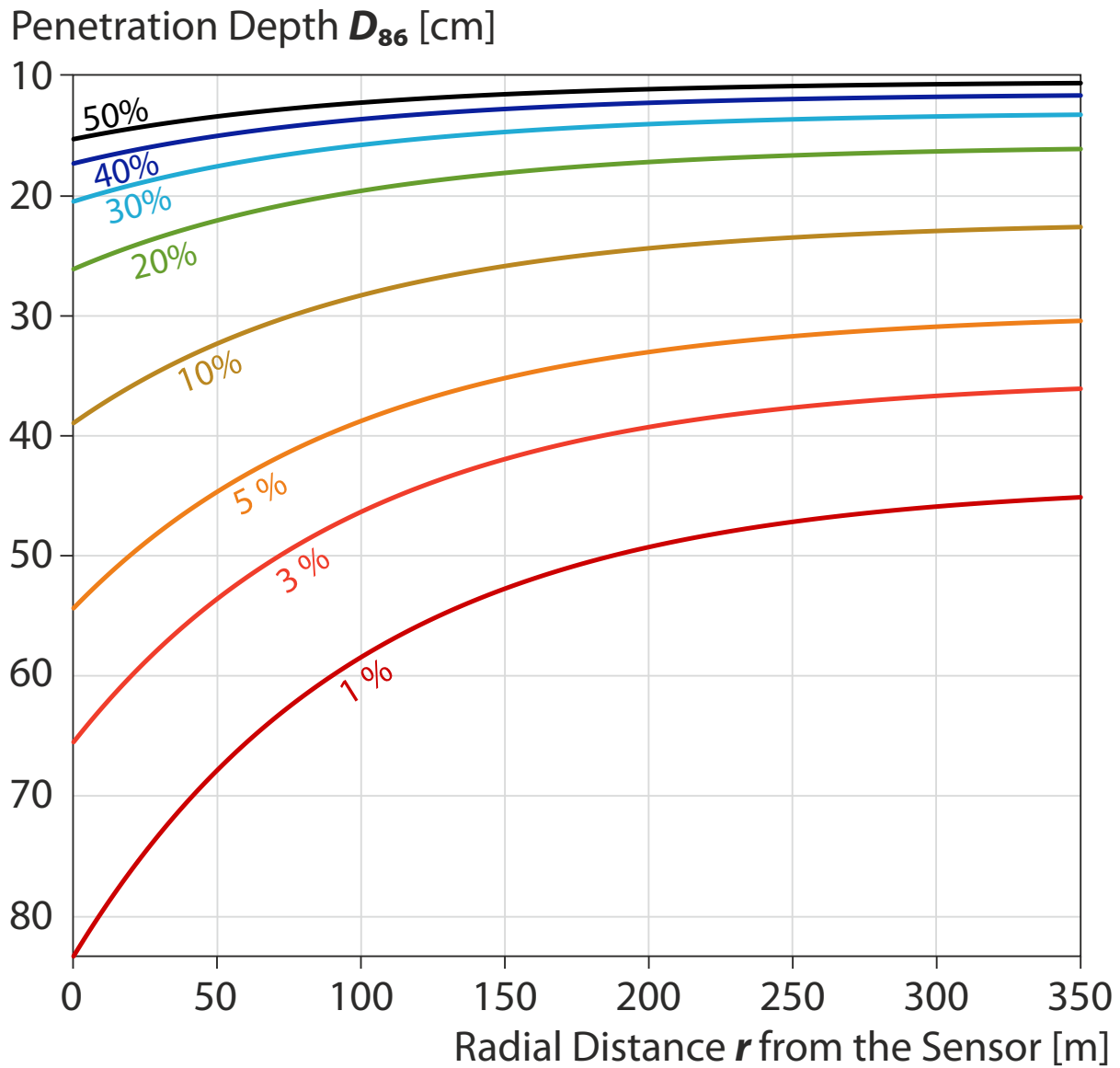


Figure 8. Dependency of the penetration depth D_{86} (eq. 8) on radial distance r to the sensor for a range of soil water contents θ (coloured). An exemplary humidity $h = 10 \text{ g/m}^3$ and soil composition according to section 3.4 is considered.

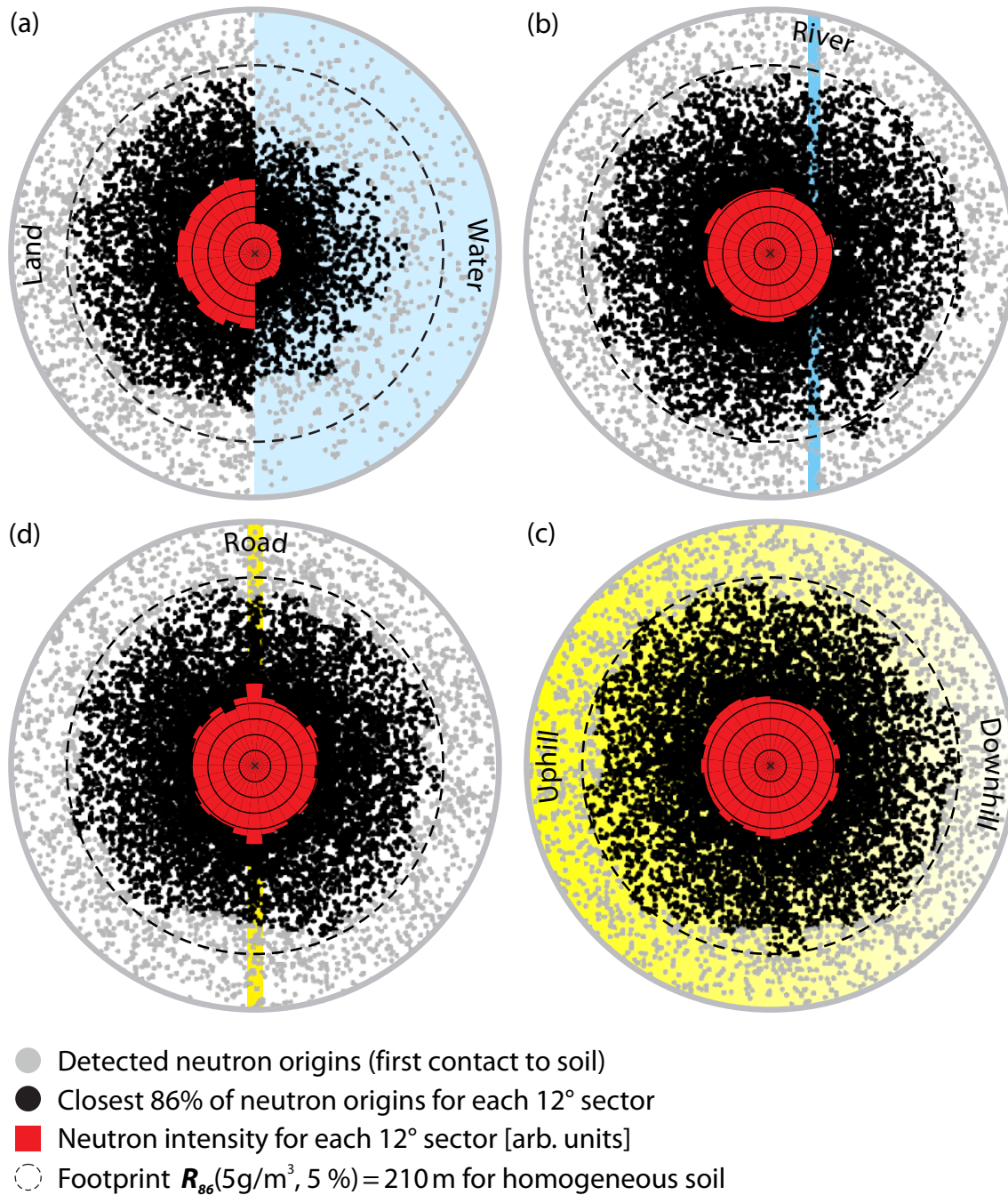


Figure 9. Anisotropy of detected neutron origins (black) and neutron intensity (red) determined for every 12° sector of a circle around a centered detector. The displayed extent is 270 m in radius, whereas the dashed line represents the isotropic footprint with radius $R_{86}(h, \theta) \approx 210$ m, considering $\theta = 5\%$ and $h = 5 \text{ g/m}^3$. The four exemplary cases illustrate bare soil (white) with (a) a coast line (blue), (b) a 10 m river at 50 m distance, (c) a 10 m concrete road (yellow) and (d) a 20% hill slope from the left down to the right.

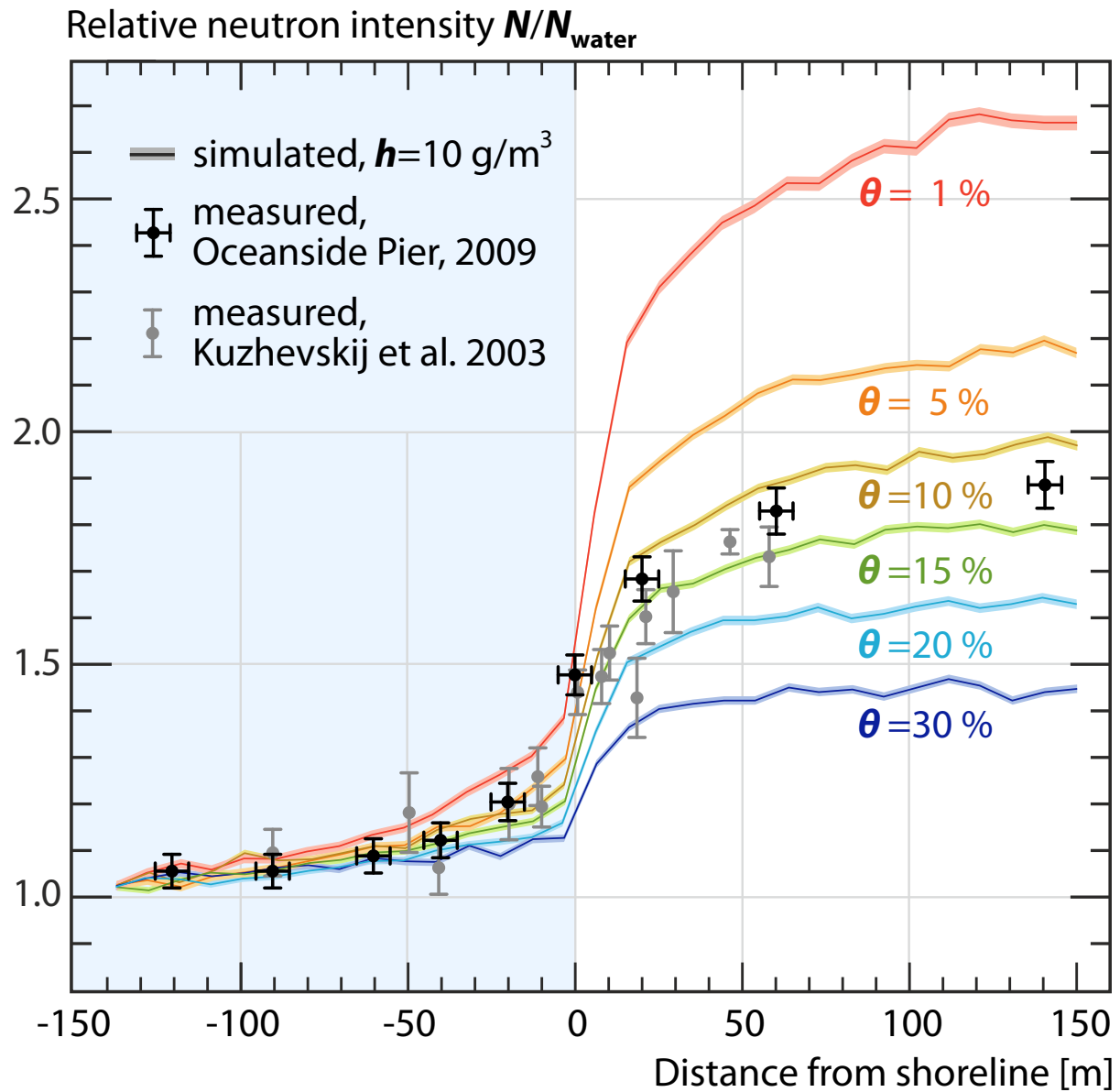


Figure 10. Coastal transect experiments simulated with a 4 m square-shaped detector every ± 10 m from the coast line. Relative neutron counts show good agreement with measurements across a water-land boundary at the Oceanside Pier (US) as well as tests at Lake Seliger (RU, from *Kuzhevskij et al. [2003]*). Air humidity h and soil moisture θ were unknown.

Table 1. Parameters for F_i (Appendix A) and D_{86} (eq. 8).

	p_0	p_1	p_2	p_3	p_4	p_5	p_6
F_1	8735	17.1758	11720	0.00978	7045	0.003632	
F_2	$2.7925 \cdot 10^{-2}$	5.0399	$2.8544 \cdot 10^{-2}$	0.002455	$6.851 \cdot 10^{-5}$	9.2926	
F_3	247970	17.63	374655	0.00191	195725		
F_4	$5.4818 \cdot 10^{-2}$	15.921	0.6373	$5.99 \cdot 10^{-2}$	$5.425 \cdot 10^{-4}$		
F_5	1383702	4.156	5325	0.00238	0.0156	0.130	1521
F_6	$6.031 \cdot 10^{-5}$	98.5	$1.0466 \cdot 10^{-3}$				
F_7	11747	41.66	4521	0.01998	0.00604	2534	0.00475
F_8	$1.543 \cdot 10^{-2}$	10.06	$1.807 \cdot 10^{-2}$	0.0011	$8.81 \cdot 10^{-5}$	0.0405	20.24
D_{86}	8.321	0.14249	0.96655	26.42	0.0567		